NASA CR-66919

THE LASER-INDUCED COMBUSTION OF PURE AMMONIUM PERCHLORATE AND THE STRUCTURE OF ITS COMPOSITE PROPELLANT FLAMES

By: Martin Hertzberg

Prepared under Contract No. NAS 1-8767

Atlantic Research Corporation
A Division of The Susquehanna Corporation
Alexandria, Virginia 22314

for

NATIONAL AERONAUTICS AND SPACE ADMINISTRATION

ANNUAL REPORT

November 16, 1968 - November 15, 1969

THE LASER-INDUCED COMBUSTION OF PURE AMMONIUM PERCHLORATE AND THE STRUCTURE OF ITS COMPOSITE PROPELLANT FLAMES

Contract No. NAS 1-8767

to

National Aeronautics and Space Administration
Langley Research Center
Langley Station
Hampton, Virginia 23365

Chief Investigators: Dr. R. Friedman
Dr. G. von Elbe

Project Manager: Dr. M. Hertzberg

Project Scientist: Dr. E. T. McHale

Kinetics and Combustion Group
Propulsion Division
Atlantic Research Corporation
A Division of the Susquehanna Corporation
Shirley Highway at Edsall Road
Alexandria, Virginia 22314

ACKNOWLEDGEMENTS

The author is indebted to Dr. Raymond Friedman for his guidance of this program from its inception until October, 1969; for his conception and recognition of the fruitfullness of the experimental method; and for his encouragement during development of the conceptual framework within which these results are presented. The author is also grateful to the Langley Research Center of NASA for financial support, and to the project monitor Dr. G. L. Pellett for his helpful advice and assistance. He wishes also to express our appreciation to Mr. Richard Lee for his patient and steady assistance in the development and operation of the experimental equipment, and in the analysis of data. Mr. Elmer Williams designed and developed the probe positioning system. Mr. Kenneth Clark designed, developed and fabricated the multichannel mass spectrometer recording system and provided electronic assistance as required.

TABLE OF CONTENTS

ABSTRACT

This report describes the results of a newly developed experimental method for studying the combustion behavior of heterogeneous solid propellants. The method uses a CO_2 laser beam to sustain low-pressure combustion from a laminarized propellant consisting of AP/fuel/AP sandwiches of millimeter slab thickness. The significant flame dimensions are expanded in size so that the flame structure is readily probed. New data are presented for the compositional, thermal and flow structure of these laser-induced flames.

These data include:

(1) The burning rate of pure ammonium perchlorate (AP) as a function of incident laser power density.

(2) The ignition delay duration for pure AP as a function of pressure and laser power density.

(3) The gas composition and flame temperature for the laser-induced AP flame.

(4) The flame structure and flow field from linearized propellant sandwiches of pure AP and polymethlmethacylate (PMM) fuel-binder.

(5) The compositional and thermal structure of the AP-PMM laser-induced flame.

These data are interpreted in the frame work of a classical wave model for the laminar combustion of a homogeneous, pre-mixed gaseous flame, which is expanded and applied to the heterogeneous combustion of a pure solid monopropellant. A solution to the conservation equation is obtained by relating the gas-phase heating rate above the propellant surface to the burning velocity of the pyrolysis gases. The solution yields regression rate predictions that are in good agreement with the data for pure AP and for several other pure monopropellants. The theory was modified to include non-adiabatic effects such as externally applied laser radiation. The data ((1) and (2) above) are in good agreement with the non-adiabatic theory.

Many previous investigations have recognized that the composite propellant problem is complicated by an effect that is absent for pure monopropellants: namely, the interdiffusion process, which tends to limit the rate for composites where fuel and oxidizer are not molecularly premixed (as they are in pure monopropellants). For such composites, the significant factor in determining the degree of premixidness is the particle size distribution. These complexities were clearly indicated by previous investigators, in their studies of the structure of quenched surfaces of composites. The new data presented in this report [(4) and (5) above] now clearly reveal the gas-phase structure of the fuel-oxidizer interdiffusion flame. A new conceptual approach is evolving by which the pure monopropellant theory is modified so that it includes the limiting effect of this diffusion process, and is thereby applicable to real composite systems. This approach yields a closed-form algebraic solution to the steady-state problem that is remarkably accurate in predicting the observables: the absolute magnitude of the composite burning rate, the pressure-dependence and the particle-size dependence.

Now that a more complete understanding of the steady-state problem has been attained, it is recommended that future research should explore the problem of applying this new experimental method, with its new degree of freedom, to non-steady-state, time-dependent problems of ignition, extinguishment and oscillatory combustion.

I. Introduction

This report describes the results of a new experimental approach to the problem of composite solid propellant combustion. The combustion behavior of both pure ammonium perchlorate (AP) and a composite propellant of macroscopic size, were studied by a technique which utilizes a CO_2 laser beam to supply radiant energy to the surface of a burning propellant. The heat input from an external laser source sustains the combustion process in a low pressure domain, where generally, neither the monopropellant nor the composite propellant would burn freely. The structure of these laser induced low-pressure flames are rendered large enough in size so that they are conveniently probed.

The pure monopropellant consisted of either pure single crystals or pressed powders of AP. The composite propellant consisted of oxidizer and fuel combined as parallel slabs (1-2mm thick) in a sandwich configuration. The apparatus and techniques previously developed, and described in a previous report[1], were modified and improved during the course of this second year's effort.

The three significant structural elements of the composite flame that were measured were: the temperature field, the compositional field of interdiffusion and chemical reaction of the fuel and oxidizer components, and the aero-dynamic flow pattern. It is generally agreed that in the absence of an experimental capability of this type little further progress can be expected in the scientific understanding of propellant combustion, but hitherto the problem has largely been regarded as not amenable to a practical solution. This is due to the fact that in an ordinary combustion environment it would be necessary to probe the field dimensions and field changes on a length and time scale of the order of microns and microseconds; and it is readily apparent that no existing method of monitoring events on such small scales are readily available. It was therefore necessary to develop an apparatus and system whereby a combustion environment could be established in which the length and time-scales were sufficiently large to accommodate microprobes of a technically feasible size.

Now a normal combustion environment for typical ammonium perchlorate propellants composed of particles in the micron range, involves rapid regression rates (0.5 to 2.0 cm sec $^{-1}$) at pressures in the range 10-100 atm. Under these conditions, vaporization of the solid is maintained by conductive heat feedback from a gas flame, whose distance above the surface is also in the micron range. As indicated above, it is usually impossible to miniaturize analytical probes to the micron size scale of such flames, and hence the structure of these propellant flames has heretofore been a matter of conjecture.[2,3,4] As pressures diminish, the flame zone thickness of premixed flames increases, so that probing of their structure is more feasible at lower pressures. However, the burning rate diminishes correspondingly because the temperature gradient above the surface decreases as the flame zone thickness increases. Thus fewer propellants are capable of burning freely at lower pressures. Even for those propellants that sustain combustion at low pressures, the particle radii are usually so small that the characteristic diffusion length is still of microscopic size. If one attempts to increase the particle radii so that the diffusion length increases, to become comparable to the premixed flame zone thickness, the propellant will no longer burn freely, and will extinguish at some particle radius at which the diffusion length is still too small for convenient probing.

These scaling problems can be resolved rather neatly by using an external radiant laser source to sustain and to control the surface regression rate. This new experimental approach allows the experimenter to control and to vary, externally, the heat input to the burning surface, <u>independent of the ambient pressure</u>. This new degree of freedom permits the experimenter to study combustion processes at lower ambient pressures than normally possible. At these lower pressures, the premixed flame zone thickness is expanded in size. Furthermore, the particle radius can now be of macroscopic size and the sample will still continue to "burn" because the laser source maintains the required heat input. Thus the diffusion length can also be expanded in size so that the interdiffusion flame is readily probed.

The net effect of using a laser source on large "radius" propellant-binder sandwiches at low pressures is to generate a macroscopic, laser-induced diffusion flame structure that is of millimeter size. This laser-induced flame is geometrically similar in structure to the flame above typical propellants of smaller particle size burning at higher pressures. In effect, this method scales the structure linearly with the gas kinetic mean free path, which increases by two orders of magnitude as the pressure decreases by two orders of magnitude. The kinetic and transport time scales are expanded in proportion so that the regression rates for the laser-induced flames are two orders of magnitude slower [.02 to .04 cm sec^{-1}].

The data to be presented, and their interpretation, demonstrate the power of this new experimental method. They are illustrative of its potential for solving many other problems in combustion chemistry. The data confirm the essential validity of the ideas of several previous investigations [2,3,4] and also provided the inspiration for the formulation of a general theory of heterogeneous propellant combustion that is more quantitative and comprehensive than any heretofore presented.[5]

II. EXPERIMENTAL APARATUS

The experimental apparatus used for studying the structure of these flames was designed and fabricated during the first year of the program. The apparatus was described in detail in the previous annual report.[1] The radiant source was a high power carbon dioxide laser, output wavelength 10.6μ, obtained from the Coherent Radiation Laboratories, Palo Alto, California. Figure 1 illustrates the experimental configuration of the sampling probe and its position relative to the surface of the propellant. Radiant energy from a high power CO_2 gas laser impinges upon a sample and sustains a macroscopic flame. The structure of the flame is depicted in Figure 2. The flame structure was determined photographically by tracking micron-size alumina particles (imbedded initially in the propellant) as they emerged from the burning surface. The compositional structure was determined by a quartz probe leading to a mass spectrometer. The thermal structure was determined simultaneously by a Pt - 10% Rh thermocouple that swept across the flame. In some experiments, the probe was maintained stationary, and traversed outward from the surface as the surface regressed away from the probe. In some experiments, pure ammonium perchlorate samples were used in place of the composite sandwich.

There were several modifications of the apparatus and several improvements in the experimental techniques made during this second year of the program.

Some effort was made to design and construct a probe positioning system that permitted more precise control of the position of the probe relative to the burning surface. Photographs of this system were submitted with the first quarterly progress report. It consists of a 2" diameter polished steel ball which revolves in a vacuum-sealing teflon seat. Both ball and seat are attached to the top flange of the combustion chamber. A 3/8" hole runs through the top of the ball and contains a stainless steel tube. The upper part of the tube attaches to the mass spectrometer via flexible tubing, and the lower part attaches to the quartz probe. The stainless tube is constrained to revolve about two orthogonal axes which intersect at the center of the ball. This is accomplished by means of two knife-edge guides. Initial vertical alignment is achieved by sliding the stainless tube through the center of the ball to the proper height, and then locking it in position with a vacuum sealing o-ring seat. The ball is then tilted about a horizon-

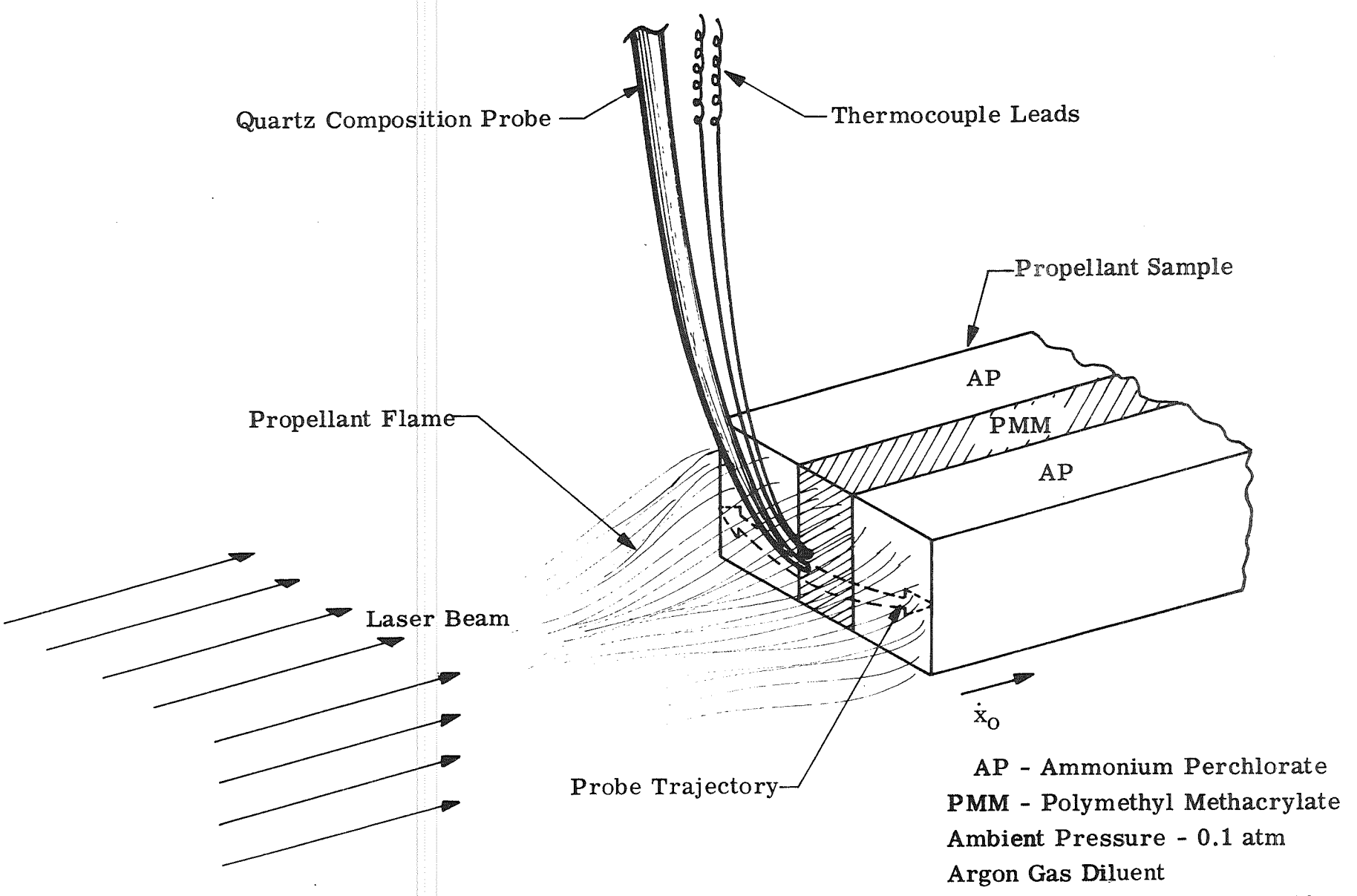

Figure 1. Probe Configuration for Studying the Structure of Laser-Induced Composite Propellant Flames.

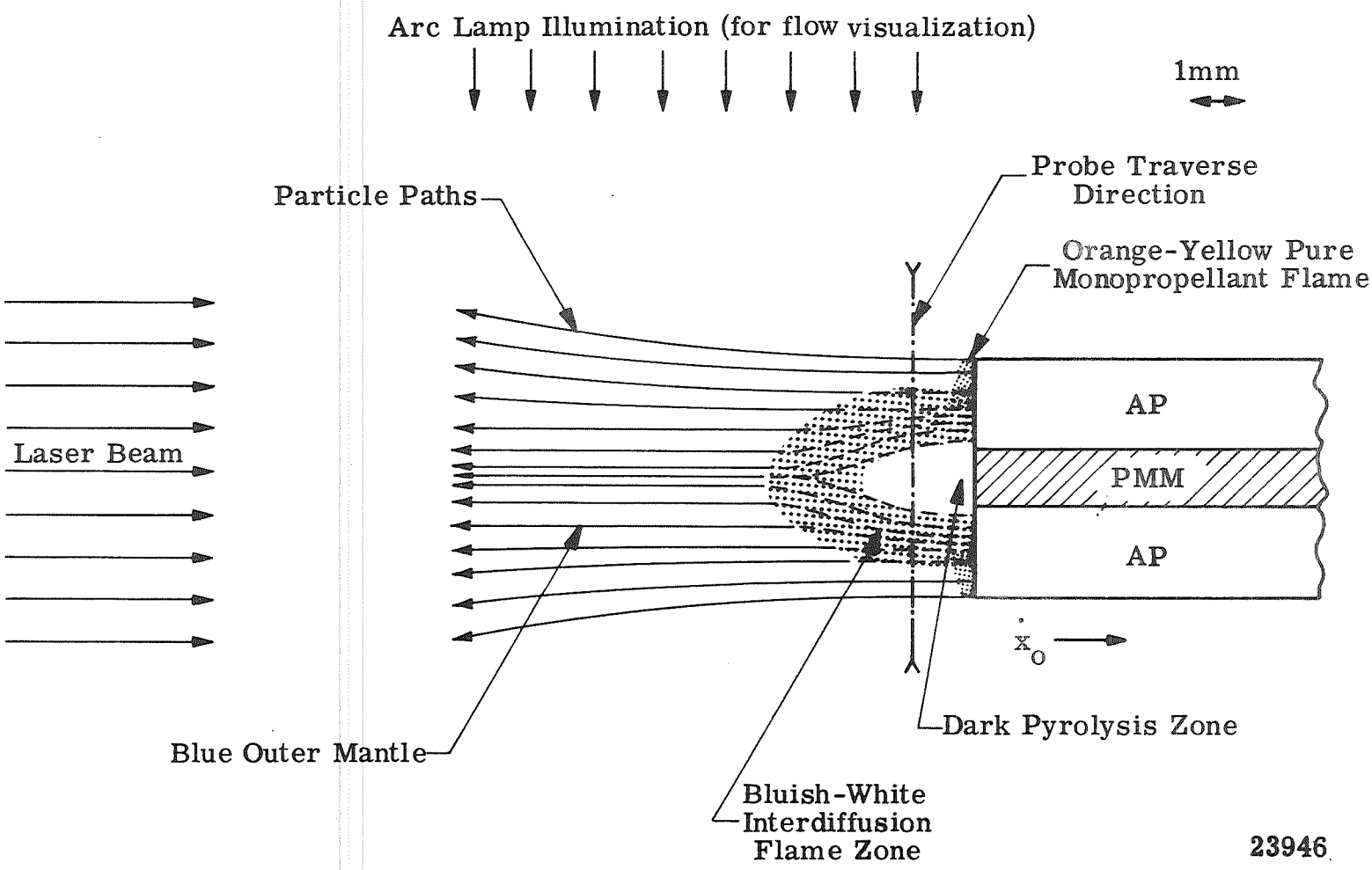

Figure 2. The Flame Structure of Laser-Induced Composite Propellant Flame.

tal axis so that the probe tip approaches the surface to a given initial distance. After ignition of the sample, the ball is then motor-driven about the other orthogonal axis so that the probe tip swings through an arc in front of the sample (as shown in Figure 1).

Improvements in the technique of flow visualization were also made during this second year's efforts, and these will be described in a following section.

A multichannel spectral recording system was designed and fabricated for use with the mass spectrometer composition probe. This system provides three simultaneous high current outputs from the electron multiplier detector of the quadrupole mass spectrometer. These three outputs are fed into three channels of a high frequency recording galvonometer. This system allows one to record the output with three separate gains (each one decade apart) for the same input current from the electron multiplier. The larger peak heights are thus read conveniently on the least sensitive scale, and the smaller peak heights are read on the most sensitive scale. This modification considerably echanced the performance of the composition probe for several of the data gathering runs during the last quarter of the program.

We now consider the geometric limits to the spatial resolving power of the probe. The bead diameters for the thermocouples used were generally 100-200μ, and it is felt that the spatial resolution of the temperature measurements are therefore of this magnitude. Thus a linear traverse across the sample of 5mm width, in effect yield 25 spatially independent bits of experimental data with which to infer the thermal structure of the flame.

Several experiments were performed in order to independently determine the spatial resolution of the composition probe. A tube was fabricated consisting of two semicircular tubular sections separated by a thin wall sheet. Argon gas was flowed through one tubular section, and nitrogen

through the adjacent tube. Both flow rates were maintained equal and parallel. The probe's spatial resolution was then measured as a function of linear sweep rate. Good spatial resolution was obtained only at the slow sweep rates. At 0.25 mm/sec; the spatial resolution was of the order of 0.5 mm. Hence a linear traverse across a sample of 5 mm width, would yield 10 independent bits of experimental data with which to infer the compositional structure. These measured spatial resolutions were of the same magnitude, although somewhat poorer, than that predicted from previous independent measurements of the sampling time constant. The measured sampling time-constant for the non-polar gases was of the order of 0.9 - 1.2 sec, which would give a spatial resolution of $\sim$0.3mm. For the polar molecules H_2O and HCl, absorption effects imposed longer time lags $\sim$2 seconds. The sampling time constant, (and hence the spatial resolution of the probe) was limited by the time required to evacuate the sampling line and to replenish it with a fresh batch of gas.

The calculated random-walk time for molecules to diffuse from the probe tip to the mass spectrometer was substantially smaller $\sim$0.2 seconds. This clearly indicates that a faster pumping speed near the probe tip could reduce the time-constant by a substantial factor, even with the existing tube length.

Naturally, a reduction in the sampling tube length would also be effective in reducing the time constant. Several orders of magnitude gain in spatial resolution could be achieved with a direct line-of-sight, molecular beam sampling system. Such sampling would also preserve the free-radical components of flame. However it was decided early in the program to defer construction of such a sampling system to a more advanced stage of the program.

III. EXPERIMENTAL RESULTS

A. Pure Ammonium Perchlorate

1. The Laser-Induced Burning Rate

Pure ammonium perchlorate normally requires a threshold pressure of 22 atm to burn freely; however, in the presence of an external radiant source it will burn at atmospheric pressure.[6] For a free-burning surface, the energy conducted to the surface is determined by the heating-rate source function. For the radiant-induced combustion, the energy absorbing through the surface can be controlled, in part, by varying the intensity of the external source. The experimentalist can thus control the energy input to the phase discontinuity and perform experiments in a constant pressure environment. This degree of freedom allows one to make additional experimental observations and thus obtain more definitive tests of the various theories. Measurements can be made, not only of the pressure dependence, but of the external radiant-flux dependence. The advantages of this experimental approach were implicitly recognized in previous experiments performed with a focussed filament-image source.[6] For these purposes, the laser source is substantially superior to previous sources.

The non-adiabatic burning rate for pressed powders and single crystals of pure AP in air (at 1 atm) were measured as a function of incident intensity. The results of these measurements are shown in Figure 3. The sample were strands of particles pressed to near crystal density or single crystals. The data points represent many individual experimental runs. The spread in the data points was caused by several factors: Errors in measuring the total source power, errors in determining the spatial distribution of the source intensity, random variations in the intensity distribution, and inaccuracies in the sample alignment.

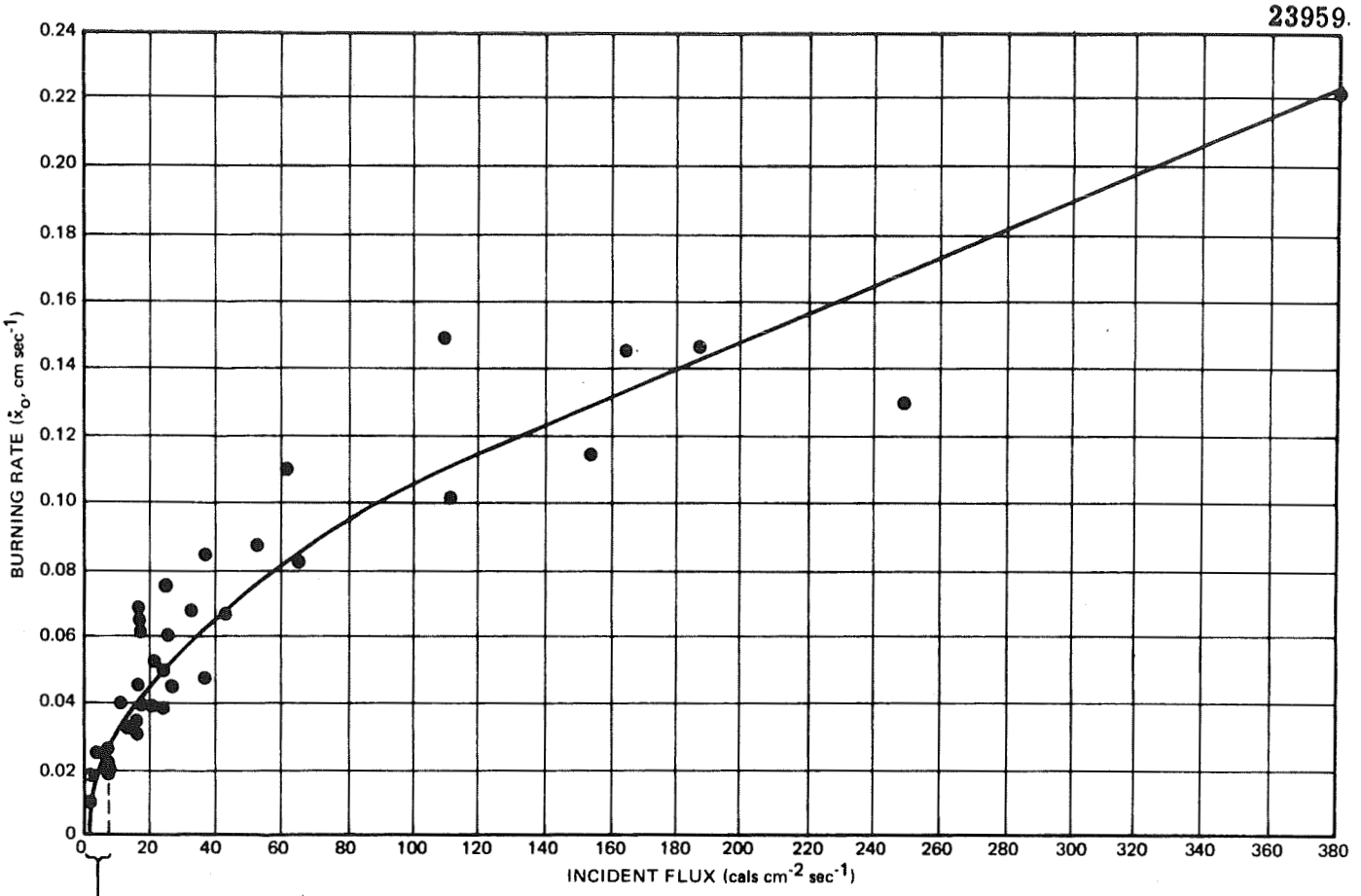

Burning Rate Versus Incident Flux, Power Density

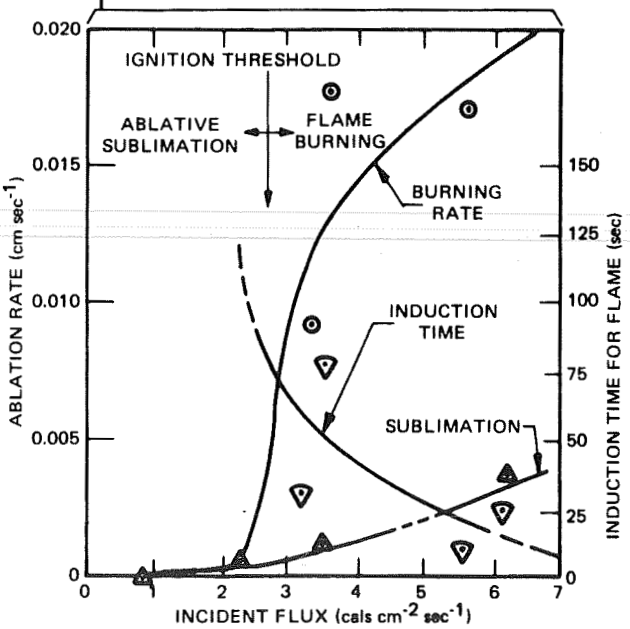

Induction Time, Burning Rate and Sublimation Rate Versus Incident Flux Near Ignition Threshold.

Figure 3. Laser-Induced Combustion of Ammonium Perchlorate (In Air at One Atmosphere, Laser Wavelength is 10.6μ).

The measured ignition threshold at 2.8 cals cm^{-2} sec^{-1} is the minimum intensity required to ignite the surface with a clearly visible flame. Above this threshold the sample burns readily with a visible flame, while below this threshold, the sample slowly sublimes (recondensing on the cold surroundings).

The previous measurements[1] were limited to relatively low power levels. Previous estimates of the heat-feedback to the surface at the free-burning threshold rate, had been obtained from a linear extrapolation of the data points in the low flux range below 30 cals cm^{-2} sec^{-1}. The newer data in Figure 3 show substantial curvature in this flux range. Because of this curvature, the previous estimate was too low by a factor of four. These measurements indicate that the total energy flux required to sustain a threshold burning rate of 0.25 cm sec^{-1} is 440 cals cm^{-2} sec^{-1}. [See reference (5) for a more detailed discussion of this question.]

2. Ignition Delays For the Laser Induced Combustion

The region near the ignition threshold of Figure 3a is magnified in Figure 3b. There we plot the burning rate, the ablation rate, and the induction time for the appearance of a flame as a function of laser power density. Below the ignition threshold of 2.8 cals $cm^{-2}sec^{-1}$; there is only one regression rate, which corresponds to the ablative sublimation process. Above the ignition threshold; we distinguish between the rate of sublimation prior to ignition, and the rate of burning after ignition. At ignition, there is a "discontinuous" increase in the regression rate after an induction time of the order of 70 seconds. The data obtained in Figure 3b were obtained at 1 atm in air. Similar data were obtained at lower pressures in Argon gas. The results of the measurements are shown in Figure 4. There we plot (the solid curves) the lines of constant induction time for ignition, as a function of pressure and laser power density.

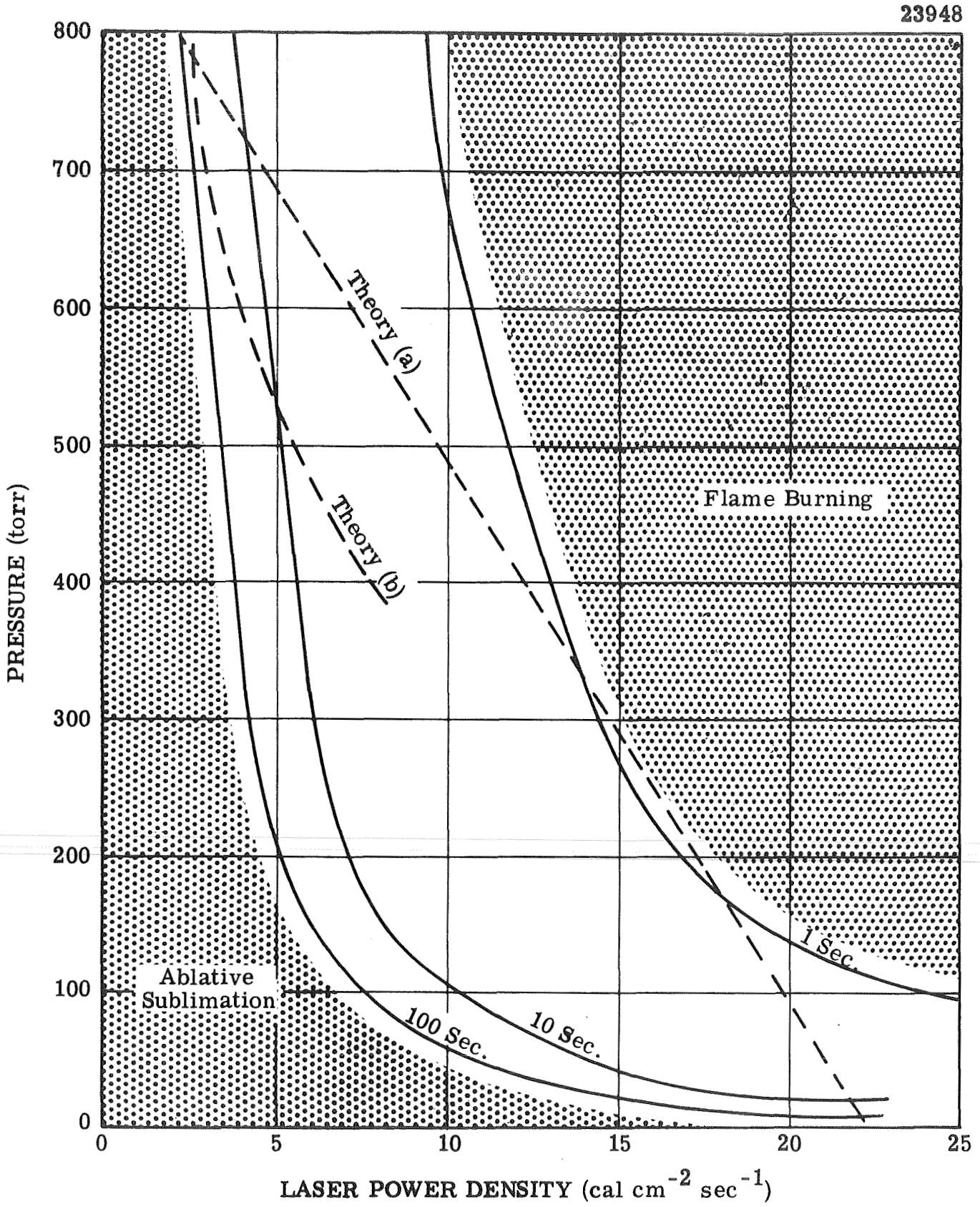

Figure 4. The Ignition Delay for the Laser-Induced Combustion of Ammonium Perchlorate as a Function of Pressure and Laser Power Density.

The induction time for ignition is defined as the time delay between the application of the laser beam and the appearance of a visible flame. These delay isochrons (lines of constant ignition delay) exhibit a steep dependence as a function of pressure in the range above 200 torr. Naturally the curves should approach the pressure ordinate near the free-burning threshold at 1.67×10^4 torr (22 atm). At lower pressures, the curves bend toward the horizontal axis and asymptotically approach the power density abscissa. We will interpret these curves later, and show that the nearly vertical regions at high pressures are those regions where the conductive heat feedback power density from the gas flame above the solid, is substantially larger than the radiant power density of the laser beam. The nearly horizontal regions at lower pressures are those regions where the reverse is true. The regions of curvature at the intermediate pressures are those where both gas flame flux and laser flux are of comparable magnitude.

3. Compositional and Thermal Structure

A wide variety of experiments were performed to determine the structure of the laser-induced flame above the pure ammonium perchlorate oxidizer. If the power density and ambient pressure exceed the ignition values indicated in Figure 4, the sample will ignite and burn with a steady orange-yellow flame that is clearly visible and readily photographed. If the beam intensity is uniformly distributed along the burning surface, the flow away from the surface is normal to the surface and fairly laminar with some divergence in the flow as the product gases expand into the ambient gas. There is also generally some upward motion due to the buoyancy effect. The orange-yellow flame persists above the pure oxidizer regions even for the composite systems (as depicted in Figure 2). The glow is generally confined to the surface region, extending outward at most a distance of 1 mm or so. It appears to extend out somewhat further and to be more diffuse at lower pressures.

An example of some of the better records obtained in such experiments is shown in Figure 5. The probe is initially positioned above a sample, similar to the configuration shown in Figure 1; however, a sample of pure AP is now used, rather than a propellant sandwich. The initial partial pressures of Argon background gas was set at fixed value, (36 torr) and the laser turned on at a power density of $\sim$30 cals cm^{-2} sec^{-1}. After a given ignition delay the sample ignites and regresses away from the probe at a given rate. In Figure 5, we plot the temperature, composition and distance record obtained in such an experiment. Initially, before the laser is turned on, the temperature is ambient (300°K), and the composition probe detects mainly the peaks due to Argon diluent gas. There is some contribution from a small amount of air leaking into the chamber and from residual gases absorbed in the system. After the laser is turned on, there is an ignition delay period during which the sample merely ablates and recondenses on the cold surroundings. The Argon intensity diminshes partly because of the presence of vap rizing NH_3 and $HClO_4$: these gases presumably condense before they can be sampled. Prior to ignition, there is a small increase in the mass 17 peak, which is atributable to unreacted

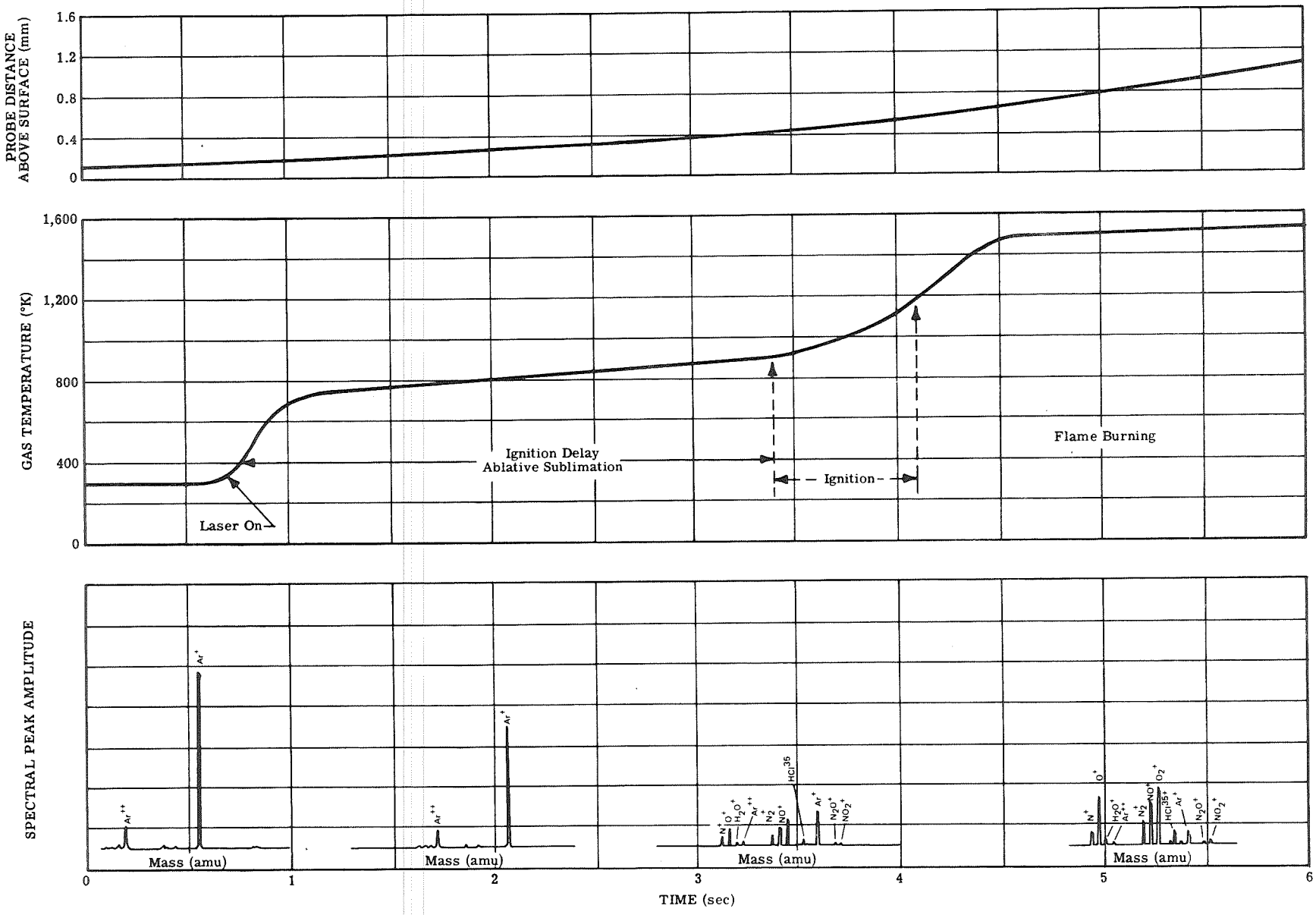

Figure 5. The Laser-Induced Combustion of Pure Ammonium Perchlorate (Experimental Record).

NH_3. Under low pressure conditions, ClO^+ and $HClO^+$ peaks [attributable to $HClO_4$ or chlorine oxide] are also detected. At ignition, the temperature increases rapidly, and the nature of the mass spectrum changes markedly.

The Argon intensity drops rapidly, limited only by the sampling time constant of the probe, and a new spectrum is established, which is now characteristic of the decomposition flame of pure AP. The temperature levels off rapidly to the laser-induced flame temperature, and the spectra are essentially unchanged thereafter, except for a small monotonic increase in Argon intensity as the probe recedes from the surface. This slow increase is caused by the diffusion of Argon gas into the AP flame.

The results of the compositional measurements obtained to date are presented in Table I. These data are revised somewhat from the data previously presented in Table I of reference 1. These revisons were based upon the sensitivity correction factors required to give proper atom balances for all the products of the final flame composition. In addition, independent measurements were made of the fragmentation patterns, of pure NO_2. The fragmentation patterns showed that the quadrupole instrument gave substantially larger NO^+/NO_2^+ ratios than those tabulated in the literature for other types of mass analyzers. These data were used to revise the NO and NO_2 abundances previously reported. The low pressure data indicate the presence of some unreacted NH_3 and $HClO_4$ and /or chlorine oxides. The measurements were obtained at various distances from the flame; however the data presented are intended to represent the composition at an average distance of about 1 mm above the surface, for an average laser power level of 10-20 cals $\cdot$ cm^{-2} $sec.^{-1}$. At higher pressures, the flame zone is very thin and very close to the surface, and only the flame products are detected. The only structure that is observed at the higher pressures is the interdiffusion of diluent Argon gas. The observed Argon dilution is about what one would calculate from simple diffusion theory. At lower pressures, where the ignition isochrons were nearly horizontal, the flame zone is apparently large enough, particularly at the ignition transient, to detect reactants and/or reaction intermediates.

These composition measurements represent the stable species in the flame; any reactive free radicals probably recombine (or react) to stable product before being sampled by the mass spectrometer. The data are compared with the equilibrium composition for the flame, and the comparison clearly reveals that the product gases still contain some untransformed chemical enthalpy.

As will be shown later, the oxidizing molecules O_2, NO, NO_2, and N_2O contain still more untransformed chemical enthalpy with respect to added fuel, and hence in the composite flame, they react still further with pyrolyzed fuel.

The results of some of the temperature measurements for the laser-induced AP flame are shown in Table II.

TABLE I

Flame Gas Composition of Laser-Induced Ammonium Perchlorate Flames (Mole Percent of Total)

	These Measurements								
Pressure (Torr)	H_2O	O_2	HCl	NO	N_2	NO_2	N_2O	Cl Oxides Cl_2 or $HClO_4$	NH_3
760	38	21	19	12	5	3	2	--	--
200	38	20	19	11	6	4	2	--	--
80	38	20	19	9	6	6	2	--	--
40	37	19	16	7	6	9	2	3	1
20	35	12	13	3	5	8	1	17	6
Calculated Equilibrium Adiabatic Composition									
760	36	29	23	--	12	--	--	--	--

TABLE II

The Preignition And Flame Temperatures For Laser-Induced Pure AP Flames

Pressure (torr)	100		36	22
Laser Flux, Cals cm^{-2} sec^{-1}	23	12	33	23
Temp. of Preignition Step (°C)	460	440	520**	460*
Temp. of Flame (°C)	1420	1220	1247	1210

* Temperature drifting slowly upward at 10°C per sec

** Temperature drifting upward at 40°C per sec

*** Data uncorrected for direct laser heating of probe, which was no larger than 50 - 100°C.

The measured flame temperatures all exceed the adiabatic flame temperature of 1100°C. The flame is clearly non-adiabatic because of the presence of the external laser source. The temperatures of the preignition step are in the range of 440-520°C. These preignition temperature measurements agree with those previously reported, and are comparable to surface temperature measurements obtained in these studies, and those of previous investigators.[1,7]

Several single-crystals that had been burned at low to moderate laser power levels were cleaved and examined microscopically. Good photomicrographs were obtained under transmitted polarized light that clearly revealed the phase-transition zone in the solid. Not enought data was obtained to warrant comparison with the results of Beckstead and Hightower.[8] The following analytic solution was obtained from the energy equation for the solid in the presence of laser absorption with a constant absorption coefficient, a (neglecting any condensed phase heat release process):

$$\frac{T - T_u}{\bar{T}_s - T_u} = \exp^{-(x_o - x)/\Delta x}(1 - \beta) + \beta \exp^{-a(x - x_o)}$$

Where: $\beta = \frac{(1 - r)\, I_o}{\lambda(\bar{T}_s - T_u)(a + \frac{1}{\Delta x})}$ and $\Delta x = \frac{\alpha}{\dot{x}_o}$

The limiting cases are:

i) $\beta \to 0$ for no incident radiant energy, or when the radiant energy is absorbed at the surface (i.e., $a \to \infty$). This gives the standard experimental surface profile with a thermal wave depth of Δx.

ii) $\beta \to 1$ for a non-reacting system with a cool surface. In this limit the temperature profile is determined by the optical absorption depth.

This transcendental equation can be solved to obtain surface temperatures from measurements of the thickness of the phase transition zone, in a manner similar to that reported by Beckstead and Hightower[8].

B. Composite Propellant Sandwiches

1. The Visible Flame Structure and The Flow Field

The flow and flame structure of composite propellant sandwich flames were depicted in Figure 2. There are clearly three distinguishable zones: First, an orange-yellow zone which is the pure monopropellant flame zone above the AP slab; second, a dark inner zone above the fuel slab which contains pyrolysis products from the fuel-binder; and thirdly a bluish white interdiffusion flame zone. There is also a bluish outer mantle of reacted fuel and oxidizer. This structure is typical of the laser-induced composite flame at pressures of 0.1 atm (76 torr) and above. At still lower pressures, the structure changes somewhat: there is no longer a well defined outer mantle, and the apex of the dark zone is no longer well defined, but appears to extend indefinitely outward.

Attempts to obtain flow patters of sandwich specimens during the previous contract period[1] generally were not successful and this prompted some current preliminary experiments to try to determine the reason. Previously the flow studies were carried out by painting a suspension of 5μ Al_2O_3 particles onto the polymer slab of the sandwich as a fine line running normal to the burning surface. It was hoped that as these propellants burned at low pressure the particles would emerge into the gas stream and would be visible under illumination. Motion pictures of these experiments, however, never showed any particle tracks. In an attempt to understand these results, the following tests were made.

A sample of polymethyl methacrylate and a single crystal of AP, both measuring a few millimeters on a side by 1-2cm in length, were painted with a suspension of 5μ Al_2O_3 particles in solvent. The particles were applied on the four sides of each sample but not on the front face. Both strands were allowed to ablate at 1 atm argon under a moderate laser flux, the surface with no particles regressing approximately 1-2mm. The samples were then examined under a microscope and it was found that the AP still had the Al_2O_3 on the four sides and none on the deflagrating face. The ablating surface of the PMM, however, was covered with particles. It could be estimated that

approximately all the Al_2O_3 that had been on the sides in the 1-2 mm thick zone that ablated had now collected on the front face. This appears to be a finding that may have implications beyond the present purpose of the experiment although no further investigation has been made. The explanation for the observed migration on the PMM is probably to be found in the fact that the polymer melts in the laser flux and the molten phase provides a fluid medium which retains melted particles and facilitates their transport. This process will not occur on AP since the oxidizer does not melt.

It was now clear that painting particles onto the polymer slab of a sandwich propellant was not the correct approach. The method of imbedding Al_2O_3 particles in AP by premixing with the oxidizer powder before strand-pressing was an obvious alternative and this has proved to be very successful. Approximately one percent by weight of added particles was found to be optimum for producing clearly visible tracks on the motion pictures of sandwich burning. External luminosity was provided by a 300-watt zirconium arc lamp which was focused onto the flame zone by a 4-inch focal length lens. [Figure 2] To date, several dozen experiments have been carried out, although many of these were to develop and improve the techniques.

The velocity profiles comprise an important component of the flame structure and will provide a test of the self-consistency of the temperature and composition profiles. Although only the overall flow patterns have been obtained thus far, it is of interest to analyze a typical run since some estimates can be made of average flow velocities in various regions of the gas. Figure 2 is a diagrammatic reproduction of a particle-containing sandwich propellant burning at 0.1 atm argon. The sample was oriented, in the actual experiment, with the two 2-mm thick strands of AP on either side of a 1.5 mm thick slab of PMM. The view of the figure is therefore looking down which is also the direction from which the motion pictures were taken; observations from the side indicated only a slight upward curvature of the flame due to buoyancy. A well-defined bluish-white diffusion flame zone surrounds a dark zone, the latter extending out from the polymer surface approximately 2.5 mm. This is roughly the distance one calculates on the basis of simple diffusion considerations.

As shown in Figure 2, the flow lines are substantially streamlined although some divergence sets in at the outside edge just beyond the visible flame zone. There are no particle tracks visible through the dark zone and the diffusion reaction zone itself is usually too bright to allow tracks to be observed. There are, however, dense tracks originating at the tip of the visible zone. These dense tracks are representative of the convergence of the flow at the apex of the pyrolysis zone. The average temperature of the dark zone, as will be shown later, is significantly lower than the average temperature surrounding it. The average molecular weight is probably also larger in the pyrolysis zone, and hence the gas density in the central dark zone is greater than outside. The laminar flow velocities would be in the reciprocal of the density ratio if the mass ablation rates of AP and PMM are the same, but since the crystal density of AP is about twice that of PMM, the mass flux of fuel leaving the surface will be only one half that of oxidizer. The gas velocities will therefore differ instead by a factor of two times the gaseous fuel/oxidizer density ratio.

In the coordinate frame of the pyrolysis products, this situation is that of a denser stationary fluid immersed in a less dense laminar stream. We can consider a stationary blunt body immersed in a laminar stream of fluid to be an analogous (although somewhat extreme) case. The flowing fluid tends to curve inward a short distance behind the blunt body, which is here represented as the dark zone. Although there is no evidence for the existence of a vortex such as would be present for the blunt body case, there is, however, substantial indication of a flow convergence around the dark zone.

2. Compositional and Thermal Structure

We now consider some representative examples of composite flame data. Several typical examples of probe traverses through the composite flame are shown in Figures 6, 7, and 8.

In Figure 6, we plot the results of a simultaneous composition and temperature traverse through the trajectory shown, at 100 torr and a flux of ∿10 cals cm^{-2} sec^{-1}. The composition and temperature data are shown in Figure 6a. The trajectory of quartz probe and thermocouple, as obtained from photographic records, are shown in Figure 6b. The horizontal scales for 6a are correlated so that the compositional and temperature data for each point along the x-axis of 6a corresponds to the position along the trajectory indicated in 6b. These data are essentially similar to the data already presented in Figure 11 of Reference 1. Now clearly, there are four types of compositional curves. Those masses that correspond to background gas peaks: Ar^{+}(40) [and Ar^{++}(20) not shown] are parabolic with minima at the center of the sample. Those mases that correspond to pyrolysis products: C_2H_2 (26), H_2 (2), and C_2H_4 (28) show maxima at the center of the sample (in the pyrolysis zone). Those masses that correspond to products of pure AP flame N_2^{+} (28), NO^{+} (30) and O_2^{+} (32) show maxima above the AP slab, and are sometimes double-peaked above each oxidizer slab. The fourth type of curve is exhibited by those masses that are products of the interdiffusion flame. For this flame, the peaks due to H_2O^{+} (18) and HCl^{+}(36) exhibit both latter types of behavior since they are products of both the pure AP flame and the interdiffusion flame. These data are clearly consistent with the visible flame structure depicted in Figure 2.

Lower concentrations of H_2O and HCl are observed in spectra 10 - 15 than in spectra 40 - 45. This is to be expected since the probe is closer to the surface in the former instance. The effect of the larger time lag for the polar molecules is corrected for by shifting both the H_2O^{+} and HCl^{+} curves approximately two spectra to the left.

In Figure 7, we present some earlier data obtained in a composition traverse very close to the regressing surface (80 torr, ∿15 cals cm^{-2} sec^{-1}). These data show substantially more hydrogen than observed in Figure 6. The geometric half width of the H_2^{+} peak is substantially wider than that of the $C_2H_2^{+}$ peak because of the larger diffusivity of hydrogen. The HCl^{+} curve peaks near the geometric center of the AP; however, the H_2O^{+} curve peaks nearly above the AP-PMM interface. This clearly indicates that the HCl observes comes mainly from the pure AP decomposition flame, whereas for the H_2O^{+} curve there is a larger contribution

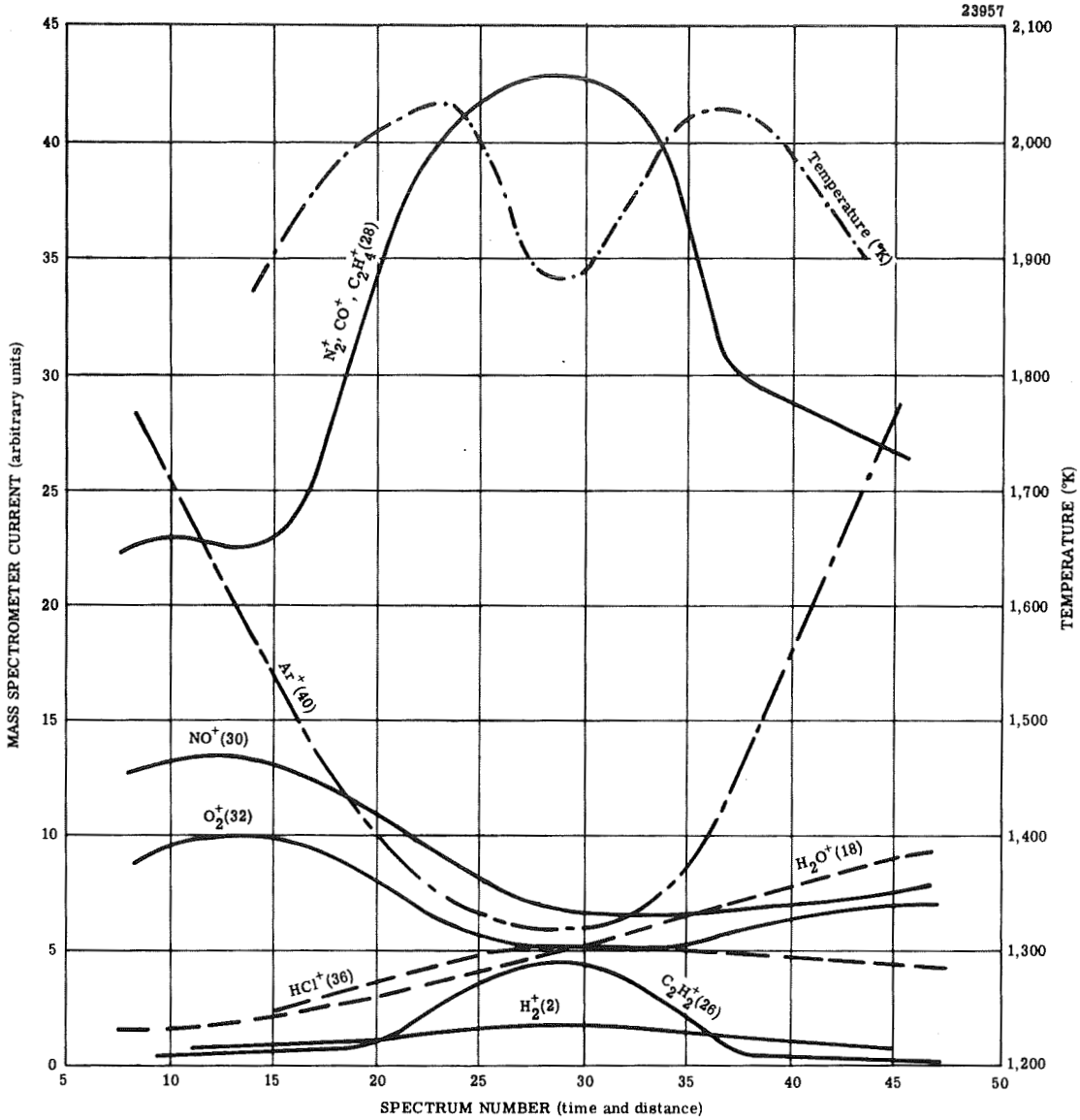

a. Composition and Temperature.

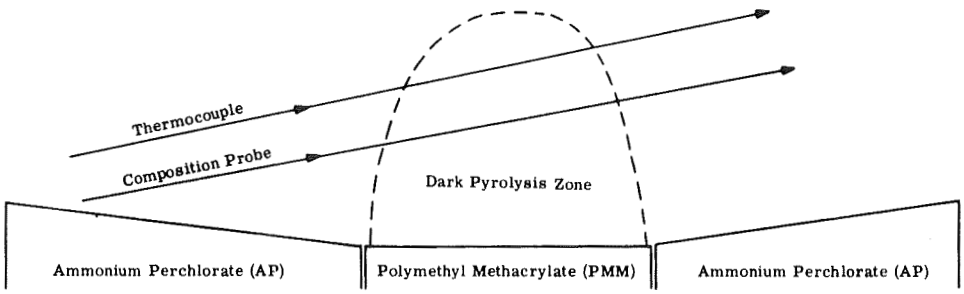

b. Probe and Thermocouple Trajectory.

Figure 6. Compositional and Thermal Structure of Laser-Induced AP-PMM Composite Sandwich Flame.

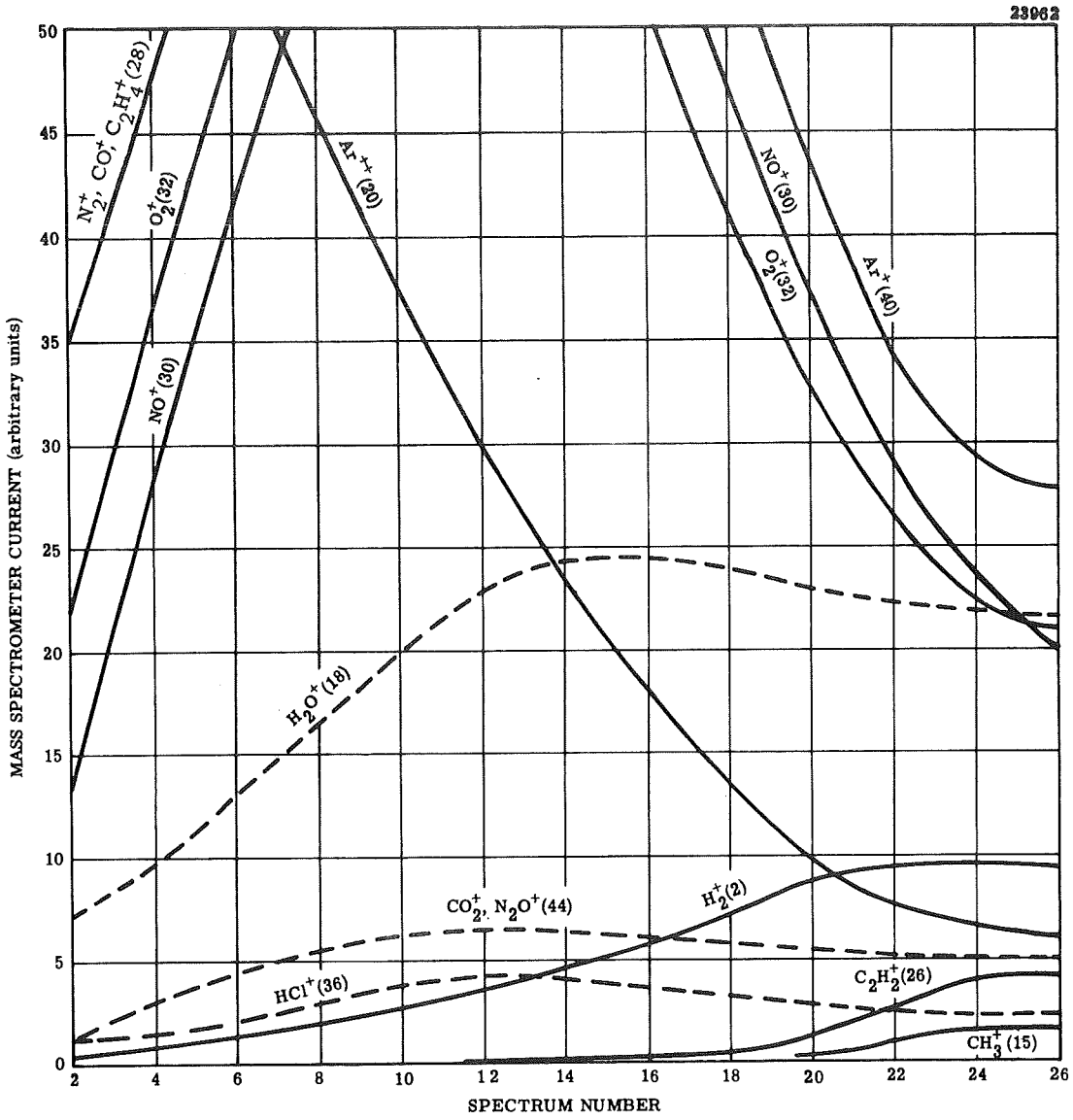

a. Composition.

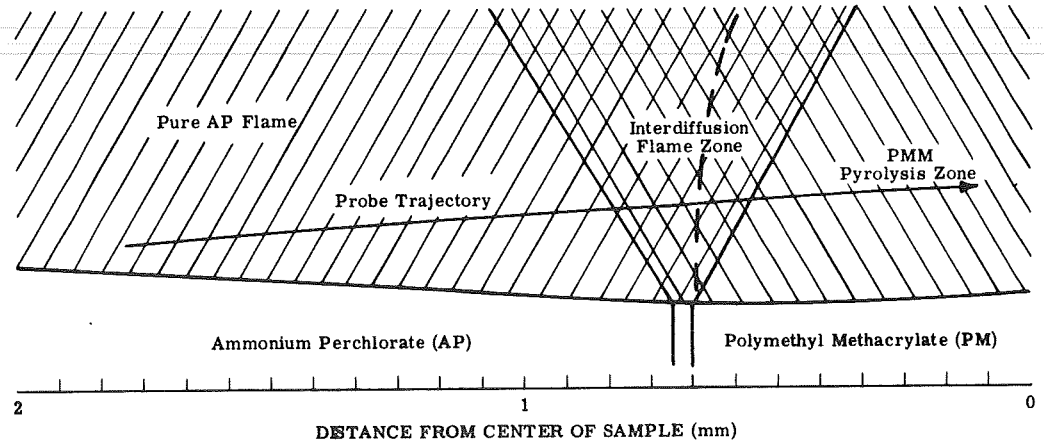

b. Probe Trajectory.

Figure 7. Compositional Structure of Laser-Induced AP-PMM Sandwich Composite Flame.

from the interdiffusion flame. The mass 44 peak is the sum of contributions from N_2O^+ and CO_2^+. The former is from the pure AP flame, the latter from the diffusion flame, hence the 44 peak shows a broad maxima starting above the AP slab and extending toward the AP-PMM interface.

In Figure 8, we present the results of a compositional and thermal traverse in which the probe was stationary in the laboratory frame and initially oriented above the PMM fuel slab. After ignition, the probe traversed outward toward the apex of the dark zone as the surface regressed away from the probe. A relatively high laser flux was used initially for ignition. After ignition, the laser power density was reduced to the lowest value consistent with maintaining a stable flame. The chamber pressure was 23 torr. The laser flux was $\sim$30 cals cm^{-2} sec^{-1} initially, and then lowered to $\sim$15 cals cm^{-2} sec^{-1} after ignition. This adjustment of the laser poser level is reflected in the temperature profile after ignition. Spectra -5 to 0 are characteristic of the preignition spectra for such samples. The peaks shown at CH_3^+ (15) and $C_2H_5^+$ (29) (and others not shown) are characteristic of the spectra of the depolymerized monomer: methylmethacrylate. Thus the composition of the preignition gases, as revealed in these experiments consists mainly of vaporized fuel monomer. These observations confirm the expectations of Shannon and Deverall,[9] that a fuel-rich mixture exists above the propellant at ignition. [In one experiment, however, a different ignition mode was observed in which the composite flame structure was preceded by the presence of the pure AP flame]. Spectra 1 - 4 of Figure 8 are associated with the ignition transient during which the monomer peaks decay, and the peaks corresponding to the composite flame structure are established. Spectra 5-23 correspond to the changes in composition and temperatures associated with the outward traverse of the probe.

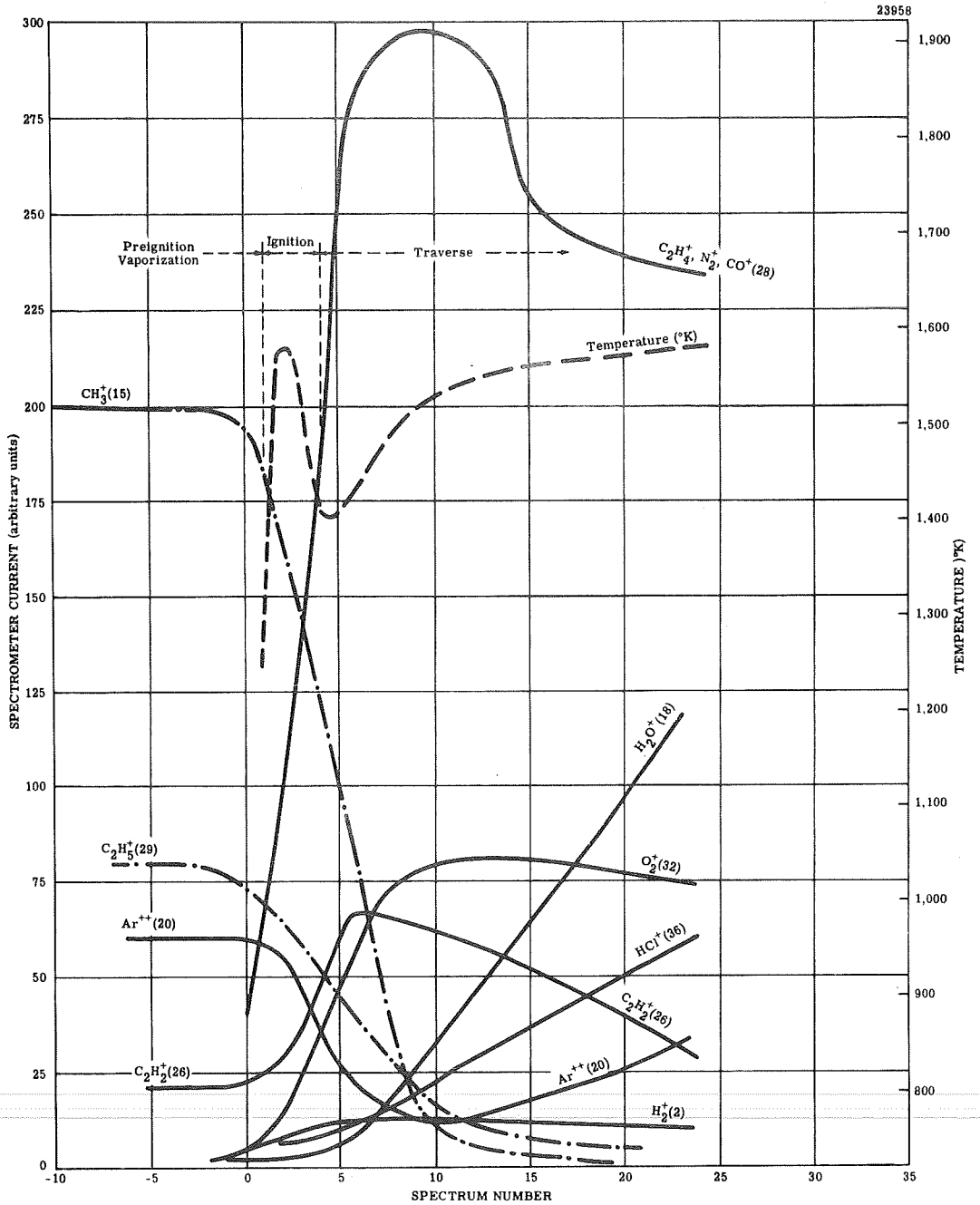

a. Compositional and Thermal Structure.

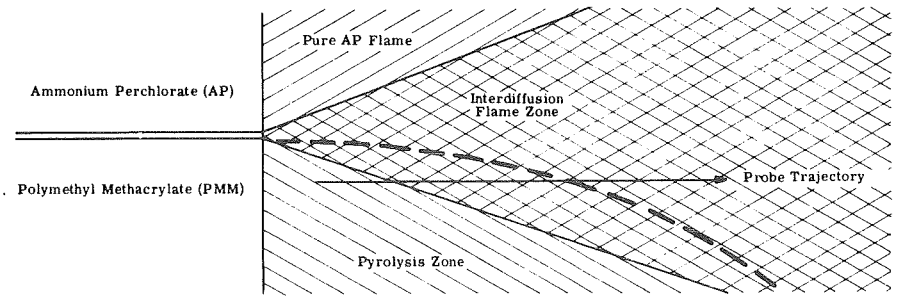

b. Probe Trajectory.

Figure 8. Compositional Structure of Laser-Induced AP-PMM Sandwich Composite Flame.

IV ANALYSIS AND INTERPRETATION

A. Pure Ammonium Perchlorate, Non-Adiabatic Theory

1. The Laser-Induced Burning Rate

The classical wave-model for the laminar, adiabatic combustion of a homogeneous, pre-mixed, gaseous flame was expanded and applied to the heterogeneous combustion of a pure solid propellant. The conservation equation for the gas, solid and Gibbsian surface states were solved and an explicit expression obtained for the steady state burning rate. The major problem of predicting the magnitude of the gas-phase heating rate, was resolved by relating the heating-rate to the burning velocity of a simulated flame above the solid surface. The theory was readily modified to include energy loss corrections for the non-adiabatic processes of conduction, convection and radiation.

The following equation was obtained by Hertzberg[10] for the non-adiabatic burning rate:

$$\dot{x}_o = \frac{v_{A\to B}[\rho_B C_B T_b' - \rho_A C_A T_p] - (I_R)_o - (I_L)_o}{\rho_x [C_B T_b - C_x T_u + \Delta H] + i(T,\alpha,\lambda)} \tag{1}$$

We assume that the observed induction time at the ignition threshold is at least equal to the time required to reach steady-state equilibrium. If we assume that $\dot{q}$ is zero below the threshold discontinuity, then the steady-state energy balance just below the threshold flux is:

$$\dot{x}_o \left\{ \rho_x [C_A T_i - C_X T_u + \Delta H] + i(T,\alpha,\lambda) \right\} + (I_L)_o = -(I_R)_o \tag{2}$$

The net radiant intensity is the difference between the incident flux and the sum of reflected and re-radiated fluxes:

$$-(I_R)_o = (1 - r)\, I - \varepsilon_s \sigma T_i^4 \tag{3}$$

The absorbed fraction of the incident energy is $(1 - r)I$. The fraction $\varepsilon_s \sigma \bar{T}_i^4$ is the re-radiated energy to the surroundings. The remainder is absorbed as latent heat, $\dot{x}_o \rho_x \Delta H$; as sensible heat $\dot{x}_o \rho_x [C_A T_i - C_x T_u]$; or is lost to the surroundings by conductive-convective processes, $\dot{x}_o i(T,\alpha, \lambda) + (I_L)_o$.

The magnitude of $\dot{x}_o$ at the ignition threshold was measured. Since that magnitude corresponds to the ablative sublimation rate at threshold, we may estimate the size of these loss terms. The energy flux absorbed as latent heat is 0.71 cals $cm^{-2} sec^{-1}$. The sensible heat term is difficult to estimate because of uncertainties in the heat capacities at the ignition temperature T_i. We use the measured value of 720 °K for T_i[11] and obtain 0.16 cals $cm^{-2} sec^{-1}$ as a reasonable estimate. The maximum re-radiated loss for unit surface emissivity is 0.37 cals $cm^{-2} sec^{-1}$. Substracting the sum of these from the incident intensity of 2.8 cals $cm^{-2} sec^{-1}$ gives a minimum of 1.5 cals $cm^{-2} sec^{-1}$ remaining for the sum of reflectance and conductive-convective losses: $rI + \dot{x}_o i(T,\alpha,\lambda) + (I_L)_o$.

We further assume that at these low burning rates $\dot{x}_o i(T,\alpha,\lambda) << (I_L)_o$. These estimates for the non-adiabatic losses, together with reasonable values for the other parameters, may be substituted into equation (1), and yield:

$$\dot{x}_o = \left\{ 14.7 + 0.62 \left[(I - 1.9)(\text{cal cm}^{-2}\text{sec}^{-1}) \right] \right\} \times 10^{-3} \text{ cm sec}^{-1} \quad (4)$$

The experimental data are compared with the theoretical prediction in Figure 9. The theory assumes that $v_{A \to B} = 0$ below the ignition threshold. Above the ignition threshold, the theory assumes that a unique value of $v_{A \to B}$ for the $NH_3/HClO_4$ flame, namely 380 cm/sec, completely characterized the laser-induced combustion process.* As can be seen, the agreement in absolute magnitude between the predicted and observed rates is generally good, considering the experimental errors and the assumptions of the theory. The theory predicts an intercept on the $\dot{x}_0$-axis of 0.013 cm sec^{-1}, which is somewhat higher than the observed intercept. The predicted slope is in fair agreement with the average slope of the experimental curve. The experimental data shows some curvature in the $\dot{x}_o$ vs. I curve; while the simple theory predicts a linear dependence.

*See reference (5) for a detailed discussion.

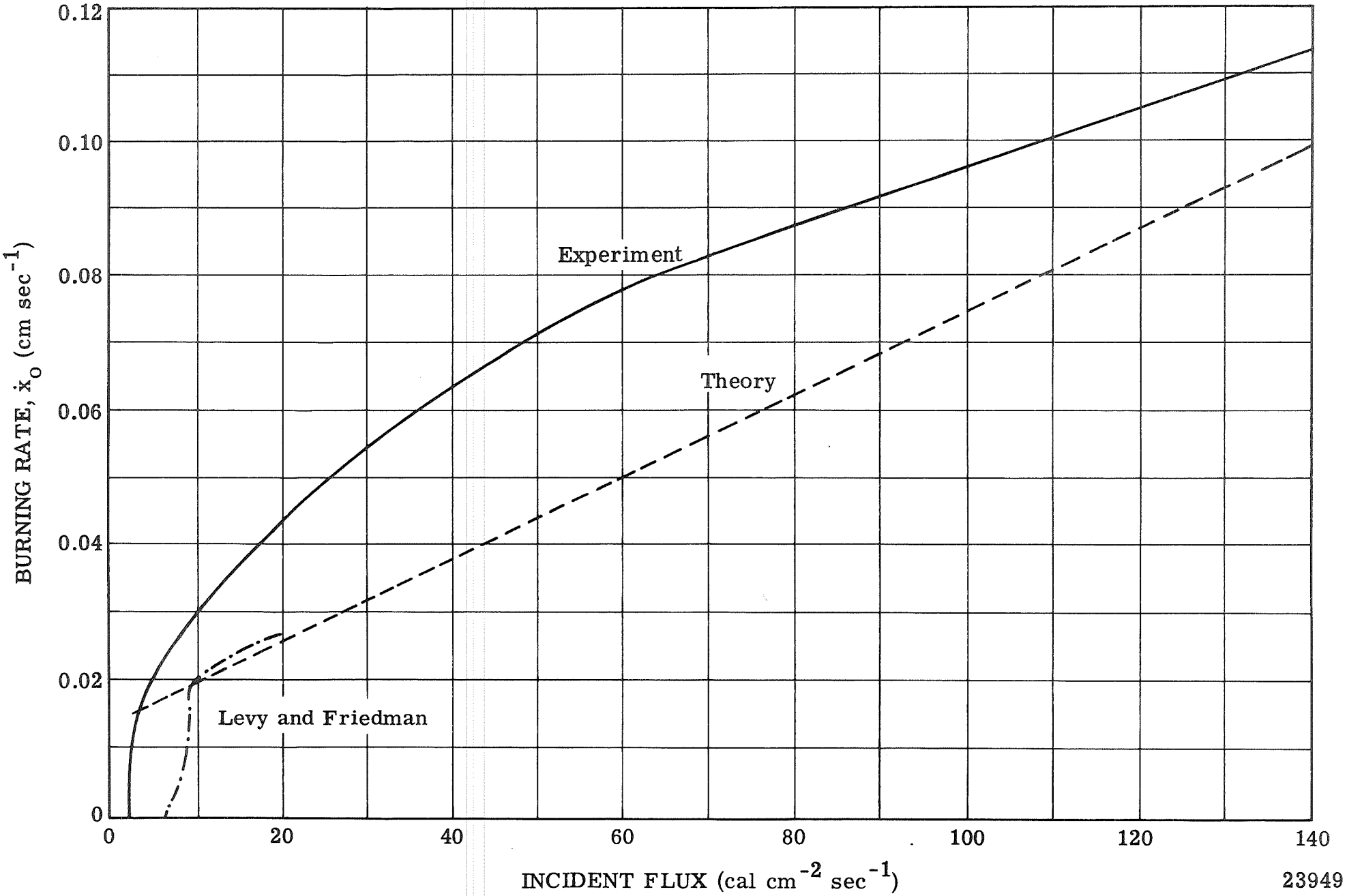

Figure 9. Laser-Inducted Combustion of Ammonium Perchlorate, Theory and Experiment.

These discrepancies may be resolved by the following considerations. The assumption of unique values of $v_{A\to B}$ and T_b' that would characterize the laser-induced combustion process at all power levels is somewhat unrealistic. It is more reasonable to assume that the properties of the A-flame ($v_{A\to B}$ and T_b') are mildly dependent on input flux I, than that they are constant, independent of flux level [see for example Table II]. We note, for example, that the observed threshold ignition temperature is 720°K, which is somewhat below the steady-state surface temperature of 830°K. If we similarly assume that the A-flame values for ($v_{A\to B}$) and the boundary-value temperatures at the ignition threshold, are somewhat lower than their free-burning steady-state values (or their higher power values), then the discrepancies are reduced. There is then better agreement between the theoretical and the observed intercept, and the theoretical curve would show some curvature near threshold.

The average measured slope compares favorably with the measured slope of Levy and Friedman[6]. Similarly the two measured intercepts are in fair agreement with each other and with the theory. The source used in these earlier studies was a focussed filament-image source with a characteristically broad spectral distribution. The previous threshold value is substantially larger, $\sim$9 cals $cm^{-2} sec^{-1}$. The difference is probably caused by the fact that the shorter wavelengths of the filament-image source were absorbed less efficiently than the 10.6μ radiation used in these experiments.

2. The Laser-Induced Ignition

We now consider the problem of ignition. For the free-laminar case, we know that a threshold pressure of 22 atm is required before an ignited sample will burn freely. Now Figure 3a shows that the minimum $\dot{x}_o$ at this threshold (0.25 cm sec^{-1}), is attained, at 1 atm, in the presence of a laser flux of 420 cals cm^{-2} sec^{-1}. The flame flux at this pressure contributes an additional 20 cals cm^{-2} sec^{-1}, so that the net energy flux into the regressing surface at the threshold rate of 0.25 cm sec^{-1}, is 440 cals cm^{-2} sec^{-1}. For the free laminar case, at 22 atm, this power density must be supplied entirely by the flame source.

Now from Figure 3a, we see that in the presence of a laser source, the threshold rate at 1 atm is 0.015 cm sec^{-1}. Assuming a linear dependence between $\dot{x}o$ and the net energy flux this corresponds to a total flux of 25 cals cm^{-2} sec^{-1}, of which only 3 cals cm^{-2} sec^{-1} is supplied by the laser source. If the additional power density supplied by the laser source at 1 atm is such a small fraction of total power density available, and if the power density from the flame varies almost linearly with pressure, why then should it require such a high threshold for an ignited sample to burn freely? Let us consider this question in more detail. We strike an energy flow balance, at 22 atm, by applying equation (1) to the threshold rate of 0.25 cm sec^{-1}. The power density absorbing as latent heat is 250 cals cm^{-2} sec^{-1}. The sensible heat term is 57 cals cm^{-2} sec^{-1}. If we assume as previously, that the non-adiabatic loss terms are burning-rate independent, they would account at most for 2 cals cm^{-2} sec^{-1}. The sum of these terms is only 309 cals cm^{-2} sec^{-1}, well below the 440 cals cm^{-2} sec^{-1} that is presumably available from the A-vapor flame source after ignition. Why, then, is not the threshold pressure substantially lower? Clearly, in order to account for the high threshold pressure, we must assume either that the non-adiabatic losses are burning-rate dependent and therefore larger than 2 cals $cm^{-2}sec^{-1}$, or that the heat feedback from the A-flame after ignition is only 309 cals $cm^{-2}sec^{-1}$, rather than 440 cals $cm^{-2}sec^{-1}$. Naturally, a combination of these two effects could be responsible.

We shall now consider, in more detail, the structure of the A-vapor flame, in order to show that a heretofore neglected kinetic factor could plausibly account for a lower heat feedback from the flame. Von Elbe and co-workers[4] were the first to suggest that a diffusional demixing effect, long observed in gas flames, could be significant for ammonium perchlorate combustion. This effect was postulated to account for the ridge-like structures observed at the surfaces of quenched single crystals samples of Hightower and Price[12]. For gas flames, this diffusional demixing effect generates a cellular flame structure. It is observed only in those premixed flames where

the mass diffusivity of a stoichiometric deficient component exceeds the mass diffusivity of the rich component. This would be the case for the NH_3-$HClO_4$ A-flame, for clearly, the flame is fuel-lean and the lighter fuel molecule has a significantly higher diffusion coefficient than the oxidizer molecule. If there is a steep dependence in the burning velocity as a function of the stoichiometric ratio (as is the case for the fuel-lean perchloric acid flames), the preferential diffusion of fuel molecules tends to reduce the burning velocity in such a way as to stabilize any slower perturbations along the flame front. The resultant effect is a cellular flame structure. For the A-flame above a solid propellant, such a cellular structure introduces gradients perpendicular to the x-direction, and has the net effect of diminishing the A-flame heat feedback to the surface.

In the A-flame, the light NH_3 molecules preferentially diffuse ahead into the burned gases and also laterally along the flame front into the surrounding inert gas. This diffusional demixing can substantially reduce the heat feedback near the edge of the sample and near the domes of the cellular flame, an effect which is not compensated for at the rims of the cells.

The phenomenon is linearly pressure dependent, the cell size being large at low pressures and small at high pressures.[12] Thus the diminished heat feedback resulting from diffusional demixing is less significant at higher pressures where the cell size is smaller. This phenomenon could account for the observed high threshold pressure limit. It also accounts for the marked stabilizing effect of small quantities of fuel additives.

We now consider the problem of the ignition threshold for the steady-state, laser-induced combustion of ammonium perchlorate at various pressures. The experimental data for the ignition threshold delays are shown in Figure 4.

If we substitute equation (3) into equation (1) and solve the resultant equation for the incident intensity I, we obtain:

$$I = \frac{1}{(1-r)} \left\{ \dot{x}_o \rho_x \left[C_B T_b - C_x T_u + \Delta H \right] - v_{A \to B} \left[\rho_B D_B T_b' - \rho_A D_A T_p \right] + (I_L)_o + \epsilon_s \sigma T^4 \right\} \qquad (5)$$

If we now substitute the previously used values for these parameters (assume a value of 0.10 for the reflectivity r), and solve for the intensity at the ignition threshold, we obtain:

$$(I)_{\text{threshold}} \ (\text{cals cm}^{-2}\text{sec}^{-1}) = 1.46 \times 10^3 \ (\dot{x}_o)_{\text{threshold}} \ (\text{cm sec}^{-1}) - 19.1p(\text{atm}) + 1.72 \qquad (6)$$

The quantity, $(\dot{x}_o)_{\text{threshold}}$, is the steady-state rate at the ignition threshold. We make the further simplifying assumption that this threshold rate is constant at the value 0.014 cm sec^{-1}, which is the height of the ignition step at 1 atm (Figure 3b). The resultant predicted ignition curve based upon these simplifying assumptions is the curve marked "Theory (a)" in Figure 4.

There is thus approximate agreement in absolute magnitude and in the overall pressure dependence. Clearly, however, the assumptions made in deriving equation (6) from equation (5), and the further assumption of a constant $(\dot{x}_o)_{\text{threshold}}$, are rather crude approximations. We know, for example, that the height of the ignition step, in the limit of zero laser power density, is much larger at higher pressures (at least 0.25 cm sec^{-1} at 22 atm). The lower pressure measurements reported by Friedman, Hertzberg, McHale, and von Elbe[1] indicate that the ignition steps are smaller than 0.014 cm sec^{-1} at pressures below 1 atm. If one assumes a variable value for $(\dot{x}_o)_{\text{threshold}}$, the theoretical curve would be steeper toward the vertical at higher pressures. It would also show some small curvature at lower pressures, and would thus give better agreement between theory and experiment. The curve marked "Theory (b)" is obtained by assuming that $(\dot{x}_o)_{\text{threshold}}$ varies continuously from 0.017 cm sec^{-1} at 1000 torr to 0.011 at 380 torr. The theory could be refined still further by assuming a pressure dependence for the non-adiabatic loss terms.

The experimental data clearly indicate that the magnitude of the ignition step discontinuity diminishes with diminishing pressure. In the pressure region below 200 torr, where the curves asymptotically approach the pressure abscissa the ignition step diminishes and the rate of ablative sublimation below ignition increases (because of the higher laser power density.) In these low pressure limits, therefore, the presence or absence of a flame has a minimal effect on the steady-state regression rate. Hence there is little or no discontinuity in $\dot{x}_o$ at ignition, and the word "ignition" becomes less meaningful. It is only in the higher pressure regions, where the power density from the A-flame is large, or at least comparable to the radiant power density, that the term ignition is meaningful, and it is only in the higher pressure regions that there is a large ignition step discontinuity in $\dot{x}_o$. Clearly, the word ignition in its usual sense is a meaningful description of the physical phenomena only for the case where the presence or absence of a chemical reaction has a significant effect on the system.

Thus, the nearly vertical regions of the curves are those regions where the heat feedback power density from the A-flame is much larger than the radiant power density, whereas the nearly horizontal regions of the curves are those regions where the reverse is true. The regions of sharp curvature are those where they are both of comparable magnitude.

Any detailed predictions of the absolute magnitude of the ignition delays would require the introduction of the non-steady-state conservation equations, and is beyond the scope of these considerations. The predicted theoretical curves correspond to the limiting cases where, in effect, steady-state equilibrium is achieved with an infinite ignition delay.

3. The Quasi-Laminar Diffusion and Monopropellant Flame (QLDM) Theory

The data already presented are clearly consistent with the viewpoints previously expressed by researchers such as Powling[2], von Elbe et al[4] and Summerfield and co-workers[3,13] concerning the structure of composite ammonium perchlorate flames. These data, and the experimental approach, also provided the inspiration for the development of a comprehensive and quantitative theory of composite propellant combustion. We will here first briefly sketch the method by which this theory was formulated, then present the results, and then compare the results with experimental observations.

The theory evolves logically from the previously developed laminar adiabatic theory.[1, 10] The composite theory is in effect, an extension and an application of the pure monopropellant theory, modified so as to include the limiting effect of the diffusion process. The basic approach to the theory is as follows: The combustion rate for the composite is assumed to be proportional to the rate for a pure premixed monopropellant of equivalent initial composition. The proportionality factor is the spatially-averaged heat flux for the propellant divided by the heat flux for the premixed flame. This theory is applicable to composites, such as AP propellants, which contain oxidizers that are capable of independent exothermic decomposition. This composite theory is more general than the granular diffusion flame theory of Summerfield.[3]

A somewhat simplified form of the theory leads to the following solution for the propellant burning rate:

$$(\dot{x}_o)_{QLDM} = \left\{16\left(\frac{\alpha}{\bar{r}_o}\right)^4\left(\frac{\rho_g}{\rho_g}\right)^2 \frac{1}{v_{pm}^2\,\tau_{pm}^2} + \frac{1}{16}\left(\frac{\rho_g}{\rho_x}\right)^2 v_{pap}^2\,\tau_{pap}^2 + 2\left(\frac{\alpha\,\rho_g}{\bar{r}_o\rho_x}\right)^2\left[\frac{v_{pap}\tau_{pap}}{v_{pm}\,\tau_{pm}} + 2\right]\right\}^{1/2}$$

$$+ 1/4\,\frac{\rho_g}{\rho_x}\,v_{pap}\,\tau_{pap} - 4\left(\frac{\alpha}{\bar{r}_o}\right)^2\,\frac{\rho_g}{\rho_x}\,\frac{1}{v_{pm}\,\tau_{pm}} \qquad (7)$$

The quantities v_{pap} and v_{pm} are the burning velocities for the pure AP A-flame and the premixed A-flame, respectively. The quantities τ_{pap} and τ_{pm} are the factors $\left[\frac{T_b' - T_p}{T_b - T_u + \frac{\Delta H}{C}}\right]$ for the pap flame and the premixed flame, respectively.

We substitute the following values into equation:

$v_{pap} = 425$ cm sec^{-1} † $v_{pm} = 900$ cm sec^{-1}

$\tau_{pap} = 0.18$ $\tau_{pm} = 0.66$

$\rho_x = 1.56$ gm cm^{-3}; $\rho_g = 3.41\text{x}10^{-4}p$ (atm); $\alpha_g = 0.19\,\frac{1}{p(atm)}$

This gives:

$$(\dot{x}_o)_{QLDM} = \left\{\frac{29.3}{\bar{r}_o^{\,4}p^2} + 18.4\text{x}10^{-6}\,p^2 + \frac{0.754}{\bar{r}_o^{\,2}}\right\}^{1/2} + 1.318\text{x}10^{-2}p - \frac{5.40}{\bar{r}_o^{\,2}p} \qquad (8)$$

The regression rate is in cm sec^{-1}, $\bar{r}_o$ is in microns (μ), and p is in atmospheres. The calculated values are shown in Figure 10. The curves shown were obtained from equation (8) but were corrected somewhat in order to account for the small contribution of the diffusion flame above the fuel particles. In addition, the neglect of the pressure dependence for v_{pap} in equation (8) results in an overestimate of the rate at higher pressures. Accordingly, the calculated rates at higher pressures (>100 atm) were adjusted so that they approach the limiting sum:

$$(\dot{x}_o)_{QLDM} \rightarrow 1/2\ (\dot{x}_o)_{pap} + 1/2\ (\dot{x}_o)_{QLD} \qquad (9)$$

† This value has been adjusted upward somewhat from the previously-used value so that there is exact agreement between equation (1) and the single crystal data at 22atm.

†† QLD refers to the quasi-laminar diffusion theory which applies to a propellant system in which neither fuel nor oxidizer particles are capable of independent exothermic decomposition.

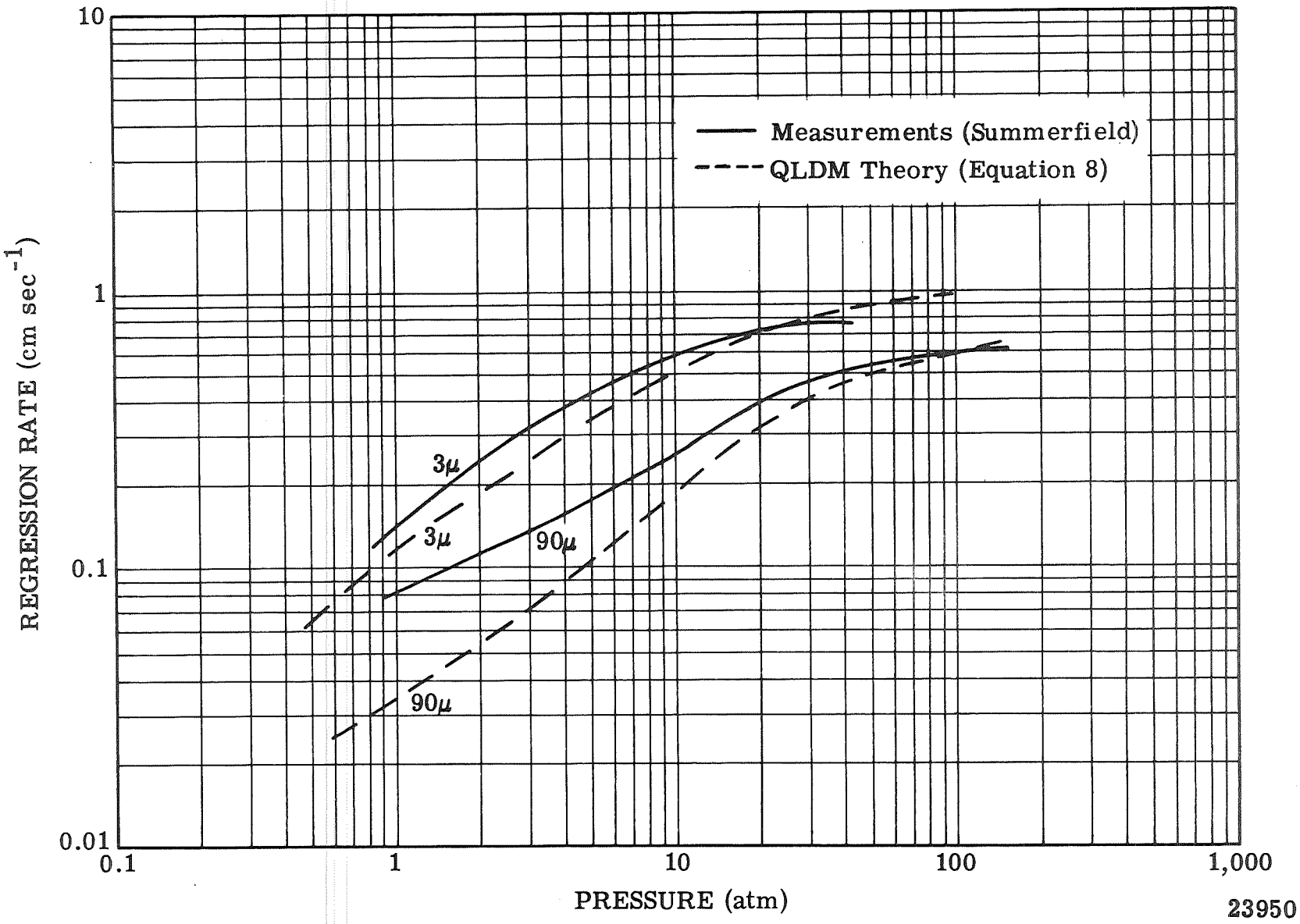

Figure 10. Burning Rate Curves for AP - Polybutadiene Epoxy Propellant [75-25] Comparison of Approximate QLDM Theory with Experiment.

The experimental data for two ammonium perchlorate propellants are also shown in Figure 10. The data are taken from the recent compilation by Steinz, Stang, and Summerfield. They are compared with the predictions of the QLDM Theory. The particle size dependence predicted by the theory is in excellent agreement with the observed particle size dependence. Similarly the pressure dependence predicted by the theory is also in good agreement with the observed pressure dependence. There is, however, only fair agreement in the absolute magnitudes. The absolute magnitudes of the measured rates are systematically larger than the theoretical predictions.

Any closer agreement would probably be surprising, considering the simplifying assumptions made in the derivation of equation (7). There are several factors that have been neglected and whose inclusion into the theory would correct for the systematic error which results in predicted rates that are generally lower than the observed rates. The simplifying assumptions that require correction are as follows: first, the assumption of equal particle size distribution for fuel and oxidizer; secondly, the assumption of a symmetric distribution of fuel and oxidizer along the surface; and thirdly, the assumption of surface planarity.

Correction for these three factors in the theory would complicate the equations further; however, their net effect would be to give better agreement between the absolute magnitudes predicted by the theory, and the observed experimental data.

V. CONCLUSIONS AND RECOMMENDATIONS

This program was the initial experimental phase of a long range program whose overall objectives were to provide researchers with improved methods of predicting propellant burning rates, combustion efficiencies, and motor transients.

The first of these objectives has effectively been attained. The physical and chemical processes that control the combustion characteristics of solid propellants have been defined and isolated. A pure monopropellant theory, which is in effect an expansion and application of the classical wave theory, has been successful in predicting the burning rate behavior of pure ammonium perchlorate. It has also been successful in predicting the laser-induced combustion rate, and the laser-induced ignition delays for AP. In addition, the same theory has been applied successfully to several other pure monopropellants: methyl ammonium perchlorate, dimethyl ammonium perchlorate, trimethyl ammonium perchlorate, hydrozonium perchlorate, ammonium nitrate and hydrazine nitroform. The following sets of A-flame velocities and boundary-value temperatures, taken from the available literature, generates predicted values for regression rates that are in good agreement with experimental measurements.

Pure Monopropellant	$v_{A\to B}$ ($cm\text{-}sec^{-1}$)	$T_b'-T_p$ (°K)	T_b (°K)	ΔH ($cals\ gm^{-1}$)
$CH_3\ NH_3\ ClO_4$	920	2400	3000	470
$(CH_3)_2\ NH_2\ ClO_4$	995	2000	2450	470
$(CH)_3\ NH\ ClO_4$	600	1500	1900	470
$N_2\ H_5\ ClO_4$	1600	1800	2300	220
$NH_4\ NO_3$	50	350	980	447
$N_2H_5C(NO_3)_3$	450	2100	2700	200

This is startling confirmation of the essential validity of the theory, especially when we remember that these data span several orders of magnitude in rate: from ammonium nitrate whose predicted steady-state rate at 5 atm is only .01 cm sec^{-1} (and hence is insufficient to maintain steady deflagration in the presence of non-adiabatic losses), to hydrazine perchlorate whose regression rate at this pressure is a rapid 1.0 cm sec^{-1}.

This theory, which is applicable to pure monopropellants whose A-flames are effectively premixed, has been extended in still another new direction. By including the limiting effect of the fuel and oxidizer interdiffusion process, a Quasi-Laminar Diffusion and Monopropellant (QLDM) Theory is obtained. This theory is applicable to composites, and is superior to previous theories in that it yields a closed-form algebraic solution for the burning rate that is remarkably accurate in predicting the steady-state observables: the absolute magnitude of the rate, the pressure dependence and the particle-size dependence. Although the theory applies to propellants that burn from a regressing surface with a laminar or quasi-laminar geometry, its extension to metallized propellants that have a non-laminar geometric components, is nevertheless readily apparent.

Thus the first of the long range program objectives has indeed been attained. It should henceforth be possible, with a reasonable estimate of the chemistry of the A-flame, and a knowledge of the thermodynamics and kinetics of the vaporization and combustion processes, to predict the laminar regression rate of any pure monopropellant. In addition with reasonable assumptions for the limiting effects of the reactant interdiffusion processes, it should also be possible to predict the rate for its composites.†

†Reference (5) contains a more detailed discussion of these questions.

The propellant burning rate is, however, only the first of the long range objectives. Other significant phenomena involve the non-steady state characteristics: motor transients, ignition behavior, and combustion instabilities. The data presented in Figure 4, and the infinite ignition delay limit predicted by equation (6), represent initial excursions into the non-steady state behavior of propellants, The experimental method that has been developed has already yielded valuable data on the ignition characteristics of propellants. These ignition studies can be readily continued or expanded to include other propellant systems. Still more meaningful and significant data could be obtained by enhancing the sensitivity of the composition probe to reactive intermediates, by diminishing the probe's time-constant, and by adding more sophisticated optical maser methods to follow the developing flame structure [14].

Since it has been possible to scale the significant dimensions of the composite flame structure in a steady-state system, it should also be possible to simulate the form of non-steady state behavior displayed in the combustion instability problem. One type of combustion instability phenomenon involves the interaction of a propellant flame with the acoustic wave pattern of rocket engine. The regressing surface and its associated flame structure interact with a pressure and flow field that vary both temporarily and spatially. The interaction of the regressing surface can be simulated by varying the spatial and/or temporal intensity of the laser beam. Thus for example, a regressing surface travelling through a standing-wave pressure peak, would in the coordinate system of the regressing surface experience a temporal increase in the heating rate source function as it approached the peak, and then a decrease in $\dot{q}$ as it recessed from the peak. This interaction is readily simulated by a temporally varying laser input $I(t)$, which would simulate the $\dot{q}(t)$ of the regressing surface. Such research could improve our understanding of the combustion instability problem.

VI. REFERENCES

1. R. Friedman, M. Hertzberg, E. McHale and G. von Elbe, "Composite Solid Propellant Flame Microstructure Determination," NASA, CR 66677 (1968).

2. Powling, J., "The Combustion of Ammonium Perchlorate-Based Composite Propellants: A Discussion of Some Recent Experimental Results, ERDE Report No. 15/R/65 (1965).

3. Summerfield, M., et al., "Progress in Astronautics and Rocketry, Vol 1, Solid Propellant Rocket Research," p. 141, Academic Press: New York (1960)

4. von Elbe, G., et al, "Chemical Kinetic and Physical Processes in Composite Solid Propellant Combustion," Atlantic Research Corporation Report NAS 1-6440, January 1967.

5. Hertzberg, M., "The Combustion of Pure and Composite Propellants, The Expansion and Application of Laminar Flame Theory to Heterogeneous Solid Propellants," (to be published) 1970, Oxidation and Combustion Reviews

6. Levy, J.B., and Friedman, R., 1962, "Further Studies of Pure Ammonium Perchlorate Deflagration," Eighth Symposium (International) on Combustion, p. 663, Williams and Wilkins, Baltimore.

7. Powling, J., "Experiments Relating to the Combustion of Ammonium Perchlorate-Based Propellants," 11th Combustion Symposium (1967), p. 447.

8. Beckstead, M.W., and Hightower, J.D., "On the Surface Temperature of Deflagrating Ammonium Perchlorate Crystals" ICRPG 3rd Combustion Conference, p. 107, (1967).

9. Shannon, L. J. and Deverall L. I., "A Model of Solid Propellant Ignition in a Neutral Environment", AIAA Journal 7 (1969), p. 497.

10. Hertzberg, M., "The Free-Laminar and the Laser-Induced Combustion of Ammonium Perchlorate," to be published in Combustion Science & Technology (1970).

11. Marklund, T., 1965, "Ingition of Ammonium Perchlorate at Different Pressures," Royal Aircraft Establishment Translation No. 1245.

12. Hightower, J.D., and Price , "Combustion of Ammonium Perchlorate," Eleventh Symposium on Combustion (1967), p. 463.

13. Steinz, J.A., Stang, P.L. and Summerfield, M., "The Burning Mechanism of Ammonium Perchlorate-Based Composite Solid Propellants," Aerospace and Mechanical Sciences Report No. 830, February 1969.

14. Schwar, M.J.R., and Weinberg ., "Laser Techniques in Combustion Research," Combustion and Flame 13, (1969), p. 335.

VII. NOMENCLATURE

α	The thermal diffusivity.
a	The absorption coefficient.
A	The chemical symbol for the gas-phase reactant(s) above the heterogeneous surface.
B	The chemical symbol for the gas-phase product(s) of the flame reaction above the surface.
C_x, C_A, C_B	Heat capacities per gram of solid (X), the reactant(s) (A), the product(s) (B).
ε_s	The emissivity of the propellant surface.
ΔH	The latent heat of vaporization per gram of solid.
$i(T,\alpha,\lambda)$	The burning-rate dependent factor for the non-adiabatic conductive-convective losses.
$(I_L)_S$	The total non-adiabatic losses from the surface-state zone (S) to the surroundings.
$(I_L)_o$	The burning-rate independent loss term.
$(I_R)_o$	The net radiant flux loss term from the surface to the surroundings.
I	The incident radiant flux.
λ_g, λ_x	The thermal conductivity of the gas and the solid.
p	The pressure.
$\dot{q}$	The heating rate per unit volume of gas flame.
r	The surface reflectivity.
$\bar{r}, \bar{r}_o$	The average particle radius.
ρ_x and ρ_g	The density of the solid and the gas.
σ	The Stefan-Boltzman constant.
τ_{pap}, τ_{pm}	The factors $\left[\frac{T_b' - T_p}{T_b - T_u + \Delta H/C}\right]$ for the pure AP flame and the premixed flame respectively.

T	The temperature.
$\bar{T}_s$	The surface temperature.
T_b	The temperature of the burned gases of the propellant.
T_p	An equivalent "preheat" temperature.
T'_b	The temperature of the burned gases of the A-flame.
T_i	The surface ignition temperature.
T_u	The initial temperature of the unburned solid.
$v_{A\rightarrow B}$	The burning velocity of pure A, preheated to the surface temperature.
v_{pap}	The burning velocity of the pure AP A-flame.
v_{pm}	The burning velocity of the premixed propellant A-flame.
X	The chemical symbol for the pure monopropellant solid.
x	The linear coordinate.
x_o	The planar surface discontinuity between S_g and S_x.
$\dot{x}_o$	The laminar regression (burning) rate.

NASA CR-66919

DISTRIBUTION LIST

NAS1-8767

	No. Copies
NASA Langley Research Center Langley Station Hampton, Virginia 23365	
Attention: Research Program Records Unit, Mail Stop 122	1 plus reproducible
Raymond L. Zavasky, Mail Stop 117	1
Dr. Gerald L. Pellett, Mail Stop 498	1
NASA Ames Research Center Moffett Field, California 94035	
Attention: Library, Mail Stop 202-3	1
NASA Flight Research Center P. O. Box 273 Edwards, California 93523	
Attention: Library	1
Jet Propulsion Laboratory 4800 Oak Grove Drive Pasadena, California 91103	
Attention: Library, Mail 111-113	1
Winston Gin, Mail Stop 125-159	1
Leon Strand, Mail Stop 125-159	1
NASA Manned Spacecraft Center 2101 Webster Seabrook Road Houston, Texas 77058	
Attention: Library, Code BM6	1
NASA Marshall Space Flight Center Huntsville, Alabama 35812	
Attention: Library	1
John Q. Miller, S&E-ASTN-PJ	1
NASA Wallops Station Wallops Island, Virginia 23337	
Attention: Library	1
NASA Lewis Research Center 21000 Brookpark Road Cleveland, Ohio 44135	
Attention: Library, Mail Stop 60-3	1
Carl C. Ciepluch, Mail Stop 500-205	1
Dr. Louis A. Povinelli, Mail Stop 6-1	1
NASA Goddard Space Flight Center Greenbelt, Maryland 20771	
Attention: Library	1
NASA John F. Kennedy Space Center Kennedy Space Center, Florida 32899	
Attention: Library, Code IS-CAS-42B	1

NASA CR-66919

DISTRIBUTION LIST

NAS1-8767

	No. Copies
National Aeronautics and Space Administration Washington, D. C. 20546	
Attention: Library, Code USS-10	1
William Cohen, Code RPM	1
Michael Gruber, Code MAL	1
Dr. Robert S. Levine, Code RPL	1
Joseph E. McGolrick, Code SV	1
Ward W. Wilcox, Code RPX	1
David L. Winterhalter, Code MAT	1
Richard J. Wisniewski, Code RMD	1
Robert W. Ziem, Code RPS	1
Air Force Office of Scientific Research 1400 Wilson Boulevard Arlington, Virginia 22209	
Attention: Code SREP	1
Air Force Rocket Propulsion Laboratory Edwards, California 93523	
Attention: Code RPM	1
Lt. C. E. Payne, Code RPMCP	1
Air Force Systems Command Andrews Air Force Base Washington, D. C. 20331	
Attention: Code SCTR	1
U. S. Army Missile Command Redstone Scientific Information Center Redstone Arsenal, Alabama 35809	
Attention: Document Section	1
Army Research Office Box CM, Duke Station Durham, North Carolina 27706	
Attention: Code CRD-AA-IP	1
Ballistic Research Laboratories Aberdeen Proving Ground, Maryland 21005	
Attention: Code AMXBR-1	1
Defense Documentation Center Cameron Station, Building 5 Alexandria, Virginia 22314	
Attention: Code OSR-1	1

NASA CR-66919

DISTRIBUTION LIST

NAS1-8767

	Copies
Johns Hopkins University Applied Physics Laboratory 8621 Georgia Avenue Silver Spring, Maryland 20910	
Attention: Chemical Propulsion Information Agency	1
R. H. Cantrell	1
T. W. Christian	1
Frankford Arsenal Propellant & Eplo. Section Philadelphia, Pennsylvania 19137	
Attention: Library, C2500-B51-2	1
Naval Air Systems Command Main Navy Building 19th & Constitution Avenue, N. W. Washington, D. C. 20360	
Attention: Code AIR-330	1
Code AIR-604	1
Code AIR-5366	1
Code AIR-5367	1
Naval Mission Center Point Mugu, California 93041	
Attention: Technical Library, Code 5632.2	1
Naval Ordnance Laboratory White Oak Silver Spring, Maryland 20910	
Attention: Library	1
Naval Ordnance System Command Washington, D. C. 20360	
Attention: Code ORD-0331	1
Code ORD-9132	1
Naval Ordnance Station Indian Head, Maryland 20640	
Attention: Technical Library, Code EDL	1
L. A. Dickinson, Code DC	1
Naval Postgraduate School Monterey, California 93940	
Attention: Technical Reports Library, Section 2124	1
Naval Research Laboratory 4555 Overlook Avenue, S. W. Washington, D. C. 20390	
Attention: Code 2027	1

DISTRIBUTION LIST

NAS1-8767

	No. Copies
Philco Ford Corporation Ford Road Newport Beach, California 92663 Attention: Library, Aeronutronic Division	1
Rocket Research Corporation 520 South Portland Street Seattle, Washington 98198 Attention: Technical Library	1
Rocketdyne 6633 Canoga Avenue Canoga Park, California 91304 Attention: Library, Deparment 086-306	1
Rohm and Haas Company Redstone Research Laboratories Huntsville, Alabama 35807 Attention: Technical Library W. A. Wood	1 1
Stanford Research Institute 333 Ravenswood Avenue Menlo Park, California 94025 Attention: Document Center for Propulsion Sciences Dr. M. Evans	1 1
Thiokol Chemical Corporation Elkton Division Elkton, Maryland 21921 Attention: Technical Information Center E. E. Hackman	1 1
Thiokol Chemical Corporation Huntsville Division Huntsville, Alabama 35807 Attention: Technical Library	1
Thiokol Chemical Corporation Reaction Motors Division Denville, New Jersey 07834 Attention: Library	1
Thiokol Chemical Corporation Wasatch Division Brigham City, Utah 84302 Attention: Technical Library R. Reed, Jr.	1 1

NASA CR-66919

DISTRIBUTION LIST

NAS1-8767

	No. Copies
Naval Weapons Center China Lake, California 93557 Attention: Technical Library, Code 753	1
Picatinny Arsenal Dover, New Jersey 07801 Attention: Library SMUPA-VA6, Scientific & Tech. Info. Branch J. Picard	1 1
White Sands Missile Range White Sands Missile Range, New Mexico 88002 Attention: Technical Library	1
Aerospace Corporation 2400 East El Segundo Boulevard El Segundo, California 90045 Attention: Library	1
Aerospace Corporation Post Office Box 95085 Los Angeles, California 90045 Attention: Tech. Info. Central Document Group	1
Aerojet-General Corporation 11711 South Woodruff Avenue Downey, California 90241 Attention: Library	1
Aerojet-General Corporation Post Office Box 15847 Sacramento, California 95813 Attention: Technical Library, 2432-2015A J. H. Wiegand, Department 4720, Bldg. 0525	1 1
Battelle Memorial Institute 505 King Avenue Columbus, Ohio 43201 Attention: Reports Library	1
Hercules, Inc. Alegany Ballistics Laboratory Post Office Box 210 Cumberland, Maryland 21502 Attention: Technical Library T. A. Angelus	1 1
Lockheed Propulsion Company Post Office Box 111 Redlands, California 92374 Attention: Library, Department 2100, Bldg. 123 Dr. P. G. Butts, Department 2100, Bldg. 114	1 1

NASA CR-66919

DISTRIBUTION LIST

NAS1-8767

	No. Copies
United Aircraft Corporation 400 Main Street East Hartford, Connecticut 06108	
Attention: Acquisitions Library	1
D. Kuehl	1
R. Waesche	1
United Technology Center Post Office Box 358 Sunnyvale, California 94088	
Attention: Technical Library	1
R. S. Brown	1
California Institute of Technology 1201 East California Boulevard Pasadena, California 91109	
Attention: F. E. C. Culick	1
Princeton University Post Office Box 710 Princeton, New Jersey 08540	
Attention: I. Glassman, James Forrestal Campus	1
Dr. M. Summerfield, James Forrestal Campus Library	1
Air Force Systems Command Research and Technology Division Bolling Air Force Base Washington, D. C. 20332	
Attention: L. Green, Jr., Code RTGS	1
CETEC Corporation 188 Whisman Road Mountain View, California 94040	
Attention: R. Anderson	1
Rocketdyne Solid Rocket Division Post Office Box 548 McGregor, Texas 76657	
Attention: S. C. Britton	1
Brigham Young University Provo, Utah 84601	
Attention: M. D. Horton	1
Office of Naval Research Department of the Navy Washington, D. C. 20360	
Attention: R. D. Jackel, 429	1

NASA CR-66919

DISTRIBUTION LIST

NAS1-8767

	No. Copies
Stevens Institute of Technology Mechanical Engineering Department 5th and Hudson Streets Hoboken, New Jersey 07030 Attention: Prof. R. F. McAlevy III	1
Naval Weapons Center China Lake, California 93557 Attention: E. W. Price, Code 508	1
University of Utah Department of Chemical Engineering Salt Lake City, Utah 84112 Attention: N. W. Ryan	1
Bellcomm, Inc. 1100 17th Street N. W. Washington, D. C. 20036 Attention: R. Sehgal	1
Ballistic Research Laboratories Aberdeen Proving Ground, Maryland 21005 Attention: L. A. Watermeier, Code AMXBR-XAS	1
NASA Scientific and Technical Information Facility P. O. Box 33 College Park, Maryland 20740	5